DEVELOPMENT OF A NOVEL BALLOON-SHAPE ELECTROACTIVE POLYMER (EAP) ACTUATOR

by

Maryam Soleimani
Bachelor's Degree in Electrical Engineering,
Ferdowsi University, 2003.

THESIS SUBMITTED IN PARTIAL FULFILLMENT OF
THE REQUIREMENTS FOR THE DEGREE OF

MASTER OF APPLIED SCIENCE

In the School
of
Engineering Science

SIMON FRASER UNIVERSITY

Fall 2010

Approval

Name: **Maryam Soleimani**

Degree: **Master of Applied Science**

Title of Thesis: **Development of a Novel Balloon-Shape Electroactive Polymer (EAP) Actuator**

Examining Committee:

Chair: **Dr. Marinko Sarunic** **P. Eng**
Assistant Professor, School of Engineering Science

Dr. Carlo Menon **P.Eng**
Senior Supervisor
Assistant Professor, School of Engineering Science

Dr. Rodney Vaughan
Supervisor
Professor, School of Engineering Science

Dr. Ash M.Parameswaran **P. Eng**
Internal Examiner
Professor, School of Engineering Science

Date Defended/Approved: December 6, 2010

Declaration of
Partial Copyright Licence

Abstract

Mechatronic applications require actuation devices that are inexpensive, lightweight, compact and simple. In this thesis, the designing, manufacturing, modelling, and experimental characterization of a novel balloon-shape electroactive polymer actuator are presented. The proposed balloon-shape actuator (BSA) has a spherical configuration and it can provide large displacements under high compression loads. The lightweight and inexpensive proposed BSA, is analyzed in two case studies. In the first, the behaviour of a radially expanding BSA is analyzed. The large-deformation exhibited by the BSA during radial pre-straining is investigated analytically and experimentally. The electromechanical behaviour of the BSA is studied via analytical models, and simulations based on a finite element method. In the second case study, an experimental procedure is implemented to determine the relationship between the imposed electrical field and the force exerted by the BSA. The thesis is concluded by investigating the potential use of the BSA in a wireless communication application.

Keywords: Electroactive polymer (EAP), Dielectric elastomer (DE), Balloon-shape actuator (BSA), Analytical Modelling, Hyperelastic model, finite element method (FEM).

Dedication

To my beloved parents for their unconditional love and care.

Without their support, completion of this thesis would not have been possible.

Acknowledgements

I owe my deepest gratitude to my senior supervisor Dr. Carlo Menon, whose encouragement, guidance and support from the initial to the final level enabled me to develop an understanding of the subject. In addition, I would like to thank my committee members for reading this thesis and giving their useful comments.

I would like to thank the director of Engineering School, Dr. Saif, for believing in me.

This work has not been possible without the constant support of my friends in MENRVA and Control lab.

Table of Contents

List of Figures

List of Tables

List of Acronyms

BSA	Balloon-shape Actuator
DE	Dielectric Elastomer
DEA	Dielectric Elastomer Actuator
dEAP	dielectric Electroactive Polymer
EAP	Electroactive Polymer
FEM	Finite Element Method
hBSA	half Balloon-shape Actuator
NIVB	National Instrument Vision Builder

List of Symbols

ε	Dielectric Permittivity
p	Pressure
H	Thickness
ε_r	Relative Dielectric Constant of Elastomer
ε_0	Dielectric Permittivity of Vacuum
X	Distance
Y	Young's Modulus
L_0	Initial Length
V	Volt
C	Electrical Capacitance
r, θ, φ	Spherical Coordinates
B_c	Left Cauchy Green Tensor
λ	Stretch
W	Strain Energy Density Function
σ	Stress
I_1, I_2	Invariants of Deviatoric Components
μ	Shear Modulus
α	Inner Stretch Ratio
β	Outer Stretch Ratio

$\boldsymbol{A}$	Inner Radius
$\boldsymbol{B}$	Outer Radius
$\boldsymbol{S}$	Strain
$\boldsymbol{v}$	Poisson's Ratio
$\boldsymbol{u}$	Displacement

1: Introduction

1.1 Motivation and objectives

This thesis investigates the feasibility of developing a novel compact, lightweight and simple actuator. Existing conventional actuators have in fact certain drawbacks; for instance, most technologies relying upon hydraulic, pneumatic or electrical/electromechanical actuators require the use of undesirably bulky, heavy and expensive external devices [1]. On the other hand, commercial compact and miniaturized actuators have different limitations, including small actuation range and/or high cost [1]. To address this issue, smart materials including shape memory alloys (SMAs), piezoelectric ceramics and polymers, magnetostrictive materials, and dielectric elastomers (DEs) have been proposed in recent years to design novel integrated actuators [2]. These actuators have simple designs as consisting of few interacting parts. Compared with other active materials, DEs demonstrate good overall performance in terms of maximum strain and response time [2]. Planar devices [3], rollers [4], tubes [5], stacks [6], diaphragms, buckling and circular elements [7] [8] [9], helical devices [10], contractile actuators [11], and active hinges [12] are examples of DEAs that have been developed in recent years. Planar and diaphragm DEAs are easy to fabricate; however, they do not exert a noticeable amount of force when they are under compressive load conditions [3] [5]. On the other hand, it is reported that stack and roller actuators can apply fair amounts of force, although their manufacturing process is not simple [6] [4]. The focus of this research thesis is to develop a novel DEA that is lightweight, inherently

inexpensive, and can have high force-to-weight ratio. The specific objectives of this thesis are as follows:

Objective 1: Proposing a novel actuator.

Objective 2: Introducing and modelling the materials used for manufacturing the proposed actuator.

Objective 3: Modelling the electromechanical behaviour of the actuator.

Objective 4: Introducing a procedure to manufacture the proposed actuator.

Objective 5: Developing and testing the actuator in order to assess its performance.

Objective 6: Proposing a potential application of the actuator.

1.2 Thesis outline

This thesis is organized as follows:

Chapter 1 presents a concise introduction, motivations, and objectives for the work.

Chapter 2 provides a general overview of electroactive polymers, specifically DEAs. The principles of their operation are described and features of selected DEAs are presented. A brief literature review of DEA materials and their modelling is provided. Some DEA failure modes are discussed.

Chapter 3 presents the novel balloon-shape actuator (BSA) proposed in this thesis. To characterize the BSA, two case studies are investigated. In the first, the radial deformation of the BSA is studied by analytically modelling the behaviour of the actuator

when it is inflated and electrical activated. In the second case study, the behaviour of the BSA under applied compressive load is studied.

In Chapter 4, the properties of the elastomer used for manufacturing the BSA are discussed. Experimental tests are performed in tensile tests to obtain the Young's modulus of the elastomer. Three hyper-elastic models, namely the Neo-Hookean, the Mooney-Rivlin, and the Ogden model, are studied to represent the experimentally tested behaviour of the considered elastomer.

Chapter 5 presents electromechanical modelling of the BSA. Mechanical and electrical equations representing the static behaviour of the actuator are derived, considering both the nonlinear and linear behaviour of the actuator shown respectively during large and small deformations. Results of performed numerical analyses using the finite element method are also presented.

In Chapter 6, two different methods for manufacturing the BSA are presented. The first method is based on a moulding procedure whereas the second method relies on an inexpensive technique.

In Chapter 7, the experimental procedure used to quantify force that the BSA can exert is presented and discussed. Results show that the BSA actuator is capable of exerting considerable force when compressed along its radial direction.

In Chapter 8, an application of the proposed actuator in the field of wireless communication is presented. Chapter 9 summarizes the findings of this thesis.

2: Electroactive Polymers: Literature Review

Electroactive polymers can transduce electrical energy into mechanical work and, therefore, can be used as actuators [13]. These materials can be fabricated with different shapes and configurations. DEAs could be use in different fields, including robotics, aerospace [14] and biomedical [7] [11].

2.1 Electroactive Polymers (EAPs)

EAPs are a class of active polymers that can change in size, shape, or volume when they are electrically stimulated [15]. EAPs can be classified into two main categories according to their principle of operation [2]. The first category consists of Ionic EAPs, in which displacement of ions during electrical activation causes change in shape or volume; their mode of actuation is based on Coulomb forces generated by an electric field [16]. The second category consists of Electronic EAPs, in which the arising electrostatic forces lead to an electromechanical deformation of the material [17]. Representatives of each EAP types are shown in Figure 2-1.

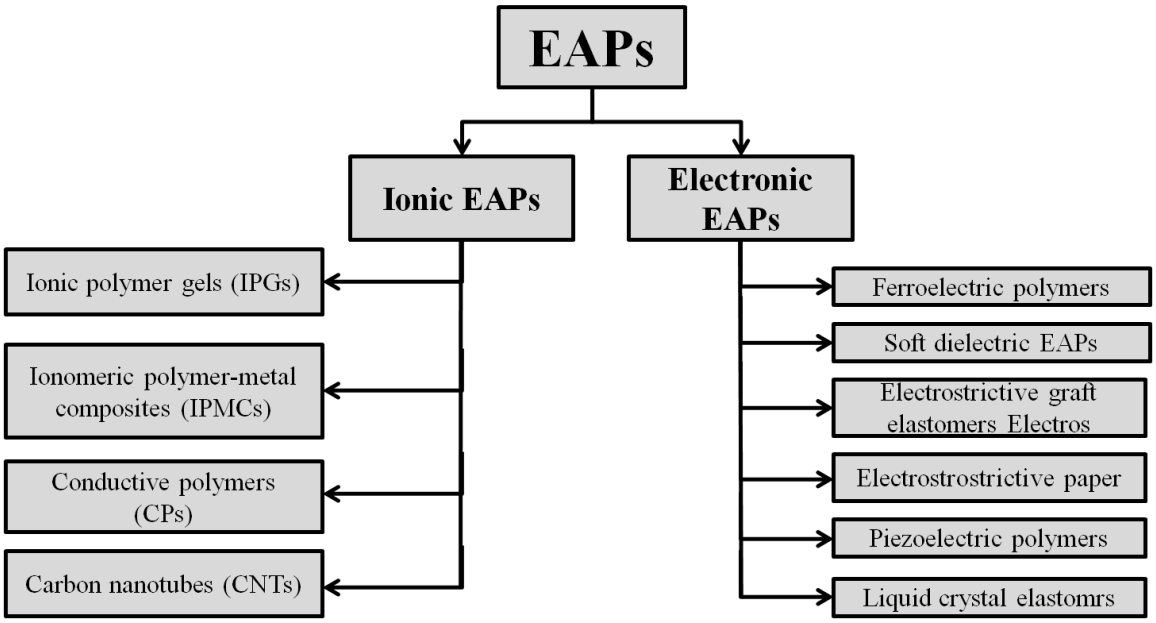

Figure 2-1: Classification of EAPs in two main groups and representing some of their selected subdivisions. This table is a modification of the table presented in [2].

One of the advantages of the Ionic EAPs is that their required activation voltage is as low as 1-2 Volts [16], [18]; however, their response time and their relaxation time are slow (seconds) compared with the Electronic EAPs (milliseconds) [18]. Low cost and high mechanical energy density are some of the advantages of Electronic EAPs, although these materials require high voltage (generally several kV) for activation [19]. The typical properties of ionic and electronic EAPs are summarized in Table 2-1.

Table 2-1: Comparison of properties of ionic and electronic EAPs (adapted from [2]).

	Ionic EAPs	Electronic EAPs
Type	Strong bending capability	Large in-Plane Deformation
Operational Condition	Wet Actuators	Dry Actuators
Activation Voltage	Low (few volts)	High (several kilo volts)
Response time	Slow (Sec)	Rapid (m Sec)
Active Stresses	Low	Large
Components	Expensive	Cheap
Strain/Stress Against an External Load	Does not hold under DC activation	Maintained under DC activation

This thesis focuses on a specific kind of Electronic EAPs known as field-induced soft dielectric elastomers (DEs). DEs can achieve an active strain of up to 380%, and a blocking stress of up to 8.2 MPa under activation [2]. Low cost, low density, high compliance, and relatively high forces [20] are attractive properties of DEs, making them the preferred choice for developing the BSA proposed in this work.

2.2 Principal operation of dielectric elastomer actuators (DEAs)

A dielectric elastomer actuator consists of a thin layer of polymer sandwiched between two compliant electrodes. When a high electric field is applied to the electrodes, the opposing charged electrodes attract each other [13]. As a result, compressive and planar stresses are applied to the elastomer by charged electrodes (see Figure 2-2). Hence, the elastomer is squeezed in the direction of the thickness, *z*, and expands in a planar direction, *x* and *y* [21]. The combination of these stresses is known as Maxwell stresses [13] [22].

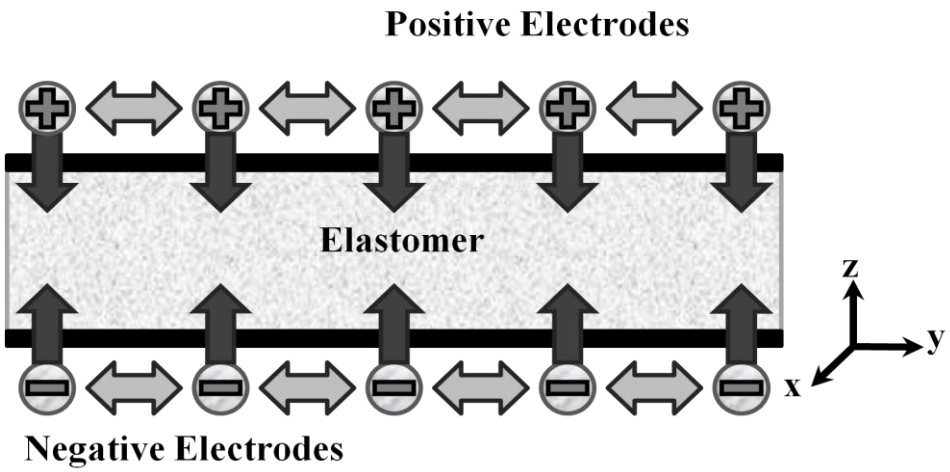

Figure 2-2: Schematic representation of compressive and planar stresses generated by charged electrodes.

When a differential voltage, *V*, is applied across the two companion electrodes, an electrostatic pressure *P*, Maxwell stress, is exerted on the polymer with thickness of *H*, which can be computed as

$$P = \varepsilon V / H^{2} \quad \textbf{(2.1)}$$

where $\varepsilon=\varepsilon_0\varepsilon_r$,

ε_r is the relative dielectric constant of the elastomer and ε_0 is the dielectric permittivity of vacuum (ε_0=8.85×10^{-12} F/m) [13]. Equation (2.1) presents an approximation of the pressure on an elastomer with uniform thickness, and it is valid for uniform electrical charge distributions.

The schematic and operating principle of a DE planar actuator under Maxwell pressure are presented in Figure 2-3.

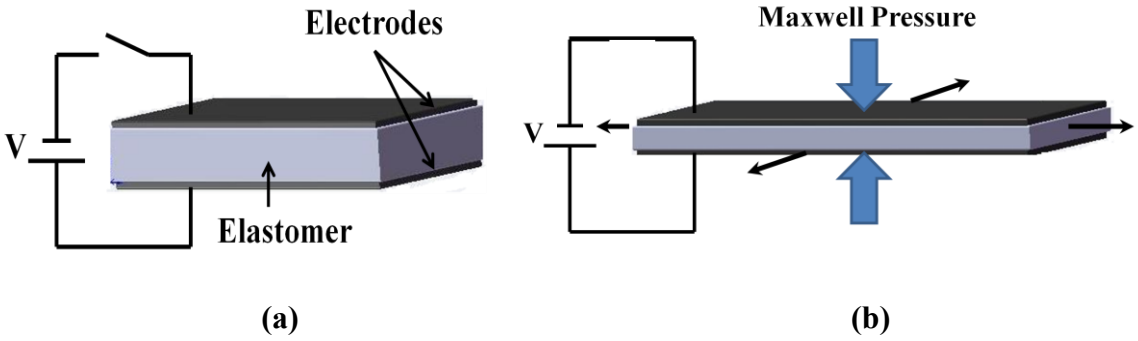

Figure 2-3: The basic unit of DEA operating principal: a) before activation b) after activation.

2.3 DEA Materials

Typically, a DEA consists of a dielectric elastomer (DE) film and two compliant electrodes. DEs generally have large relative permittivity and high dielectric strength as well as low Young's modulus in order to achieve large active strains [23].

The compliant electrodes should be as thin as possible, with good electrical conductivity and low tensile stiffness [24]. Although diverse electrode materials have been

investigated and utilized, none of them presents a clear advantage over the others, and no exhaustive theoretical study has been conducted yet to analyze their performance [25]. Some of the DEA components that have been investigated by different researchers are discussed in the following sections.

2.3.1 Elastomers

Acrylic and silicone elastomers are the most promising and widely used materials [26]. Various DEs were tested and characterized [27], [28]; particularly, many research groups have used the acrylic elastomer VHB 4910, by 3M, as dielectric material. Large active strain (over 200%), high elastic energy density (3.4 J/cm^3) [19] and high electrical breakdown strength (218 MV/m) [23] are some of its attractive properties. As a drawback however, response of the acrylic film is slower than that of silicone films, where frequencies of up to 20 kHz are possible (silicone HS3 by Dow Corning) [29], [30]. Furthermore, the acrylic film exhibits significantly greater viscous losses compared to silicone films [25]. Studies have shown that the temperature dependency of the acrylic film is much higher than for silicone films. For instance, the Young's modulus of the silicone film remained almost constant while modulus of the acrylic film decreased dramatically in the test temperature range of -50 to 75 °C [31]. In this work, we used silicone elastomer type of DE for manufacturing the BSA.

2.3.2 Electrodes

Compliant electrodes are typically made of electrically conductive particles or conductive polymers. In general, the electrode has to be selected based on the desired application because none of the proposed electrode materials was found to exhibit better performance

in all aspects. For example, graphite spray, carbon grease, graphite powder and thickened electrolyte solution were four potential electrode materials that were investigated and experimentally characterized by Carpi et al. [3], but they all had difficulty in handling electrical break down [25]. In contrast to the mentioned electrode material, gold electrodes that consist of a thin layer of beaten gold showed an attractive property called the "self-healing" effect. Preliminary tests showed that when an electrical breakdown occurred, the thin gold layer was vaporized. Because the distance between the opposing electrodes was sufficiently large to prevent any electrical breakdown, the actuator could not fail [24]. Furthermore, tests showed that the leakage currents of some tested electrodes—including carbon black, aqueous dispersions of graphite powder, and colloidal dispersion of graphite particles—were up to 3 orders of magnitude larger than those of the samples with gold leaf electrodes. However, the gold electrodes constrained the elongation of the actuator mechanically, which therefore could not deform much [25].

2.4 Literature review on the modelling of dielectric elastomer actuators

Analytical methods that account for large deformation and nonlinear elastic properties have been widely used. In this section, we review different methods for modelling and simulating a DEA actuator. In [19], various hyperelastic models were tested for tensile case in a one-dimension stress; the Ogden model gave the best performance on elastomer VHB4910 [19].

Carpi *et al.* [5] derived an analytical model for a cylindrical silicone actuator based on linear elastic theories and compared the model with experimental results that agreed with the model for a single actuator.

Kofod *et al.* [32] proposed an analytical model for a stripe actuator using Ogden strain energy function to model the elastomer. Parameters were obtained by conducting experiments in which once the strain was kept constant and force was measured, and once the load was kept constant and the strain was measured. Results showed a difference between model data and experimental data ranging from 15% to 37% in strain values for constant load case.

The behaviour of inflatable DE membranes was investigated in [33]. A model based on Ogden strain energy was used, and the material parameters were obtained by fitting test results for one-dimensional tensile test. In addition, Lochmatter [34] investigated Planar DE actuators using a hyperelastic model and fitting uniaxial tensile experiment data, and reported 10% theoretical efficiency of the actuator.

2.5 Actuators based on DE

Because DEs can be fabricated in different shapes and configurations, a variety of different dielectric elastomer actuators (DEAs) have been developed [3]- [12]. Depending on pre-straining, actuators based on soft DE can be classified into two groups: 1) actuators pre-stretched by a supporting structure, and 2) actuators not pre-stretched [18].

2.5.1 Pre-stretched DEAs

The first group shows some selected actuator configurations where the DE is pre-stretched. Reasons investigated for pre-stretching the elastomeric film include increasing the electrical breakdown strength [25], decreasing the elastomer thickness and as a result lowering applied voltage [24], and avoiding the pull-in failures—which will be discussed

in details in section 2.6. The BSA proposed here belongs to the pre-stretched DEAs category.

2.5.1.1 Diaphragm actuator

By pre-straining a coated DE, a diaphragm actuator is constructed when it is constrained by a frame, having gas pressure on one side of the diaphragm. Therefore, a buckled shape is obtained when the actuator is activated (see Figure 2-5-a), which produces a displacement of up to 50% of the diameter [8], [7] [35].

2.5.1.2 Spring Roll Actuators

These actuators can be configured to actuate in several ways, including axial extension and bending that combines both extension and bending. The biaxially pre-strained and coated dielectric film is wrapped around a compressed coil spring. Under electrical activation, the film relaxes and the actuator elongates in the axial direction (Figure 2-5-b). Free strains of up to 35% and blocking forces of up to 20 N were reported for these actuators [4]. Bending deformations become possible when the electrodes are divided into several individual active zones. The bending roll actuators can act as leg and knee joints to produce biomimetic walking [36].

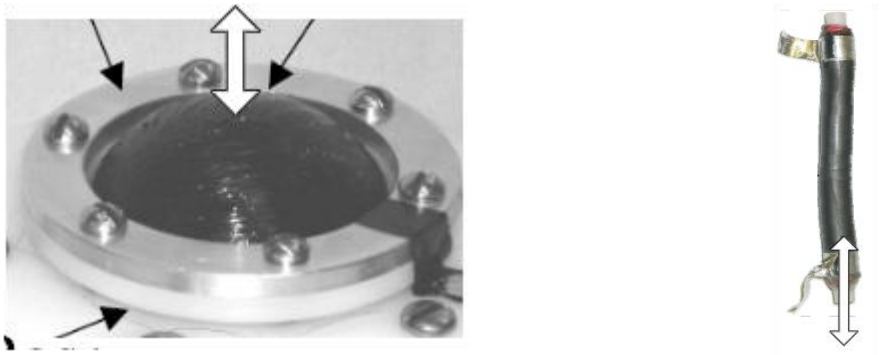

(a) (b)

Figure 2-4: Two selected actuator configurations using pre-strained DE: a) diaphragm actuator b) roll actuator adapted from [18].

2.5.2 Non-Pre-stretched DEAs

The second group does not require any support structure. The following paragraphs provide examples of non-pre-stretched DE actuators.

2.5.2.1 Unimorph actuator

The unimorph actuator consists of a planner elastomer which is longitudinally constrained on one of its two opposite coated surfaces. When the actuator is activated by an electric field, it can bend from its initial planar state toward the longitudinally constrained surface [13], [27]. Figure 2-5-a presents a schematic representation of a unimorph actuator.

2.5.2.2 Bimorph actuator

Biomorph actuators are built of at least two stacked layers of DE that can bend when one layer deforms under actuation or that can elongate when both layers actuate under an applied electric field (Figure 2-5-b) [13], [27].

2.5.2.3 Folded actuator

A folded actuator is constructed by folding one layer of dielectric elastomer several times to achieve the desired multilayered configuration. This type of actuator can provide strains of up to 15% and also exert compressive forces [6], (Figure 2-5-c).

2.5.2.4 Stack actuator

A stack actuator consists of many separate layers of dielectric elastomers with intermediate electrodes. It can take external pressure forces in the thickness direction and it provides stresses up to 20 N/mm^2 under actuation, enabling contraction along the thickness direction (Figure 2-5-d) [6] .

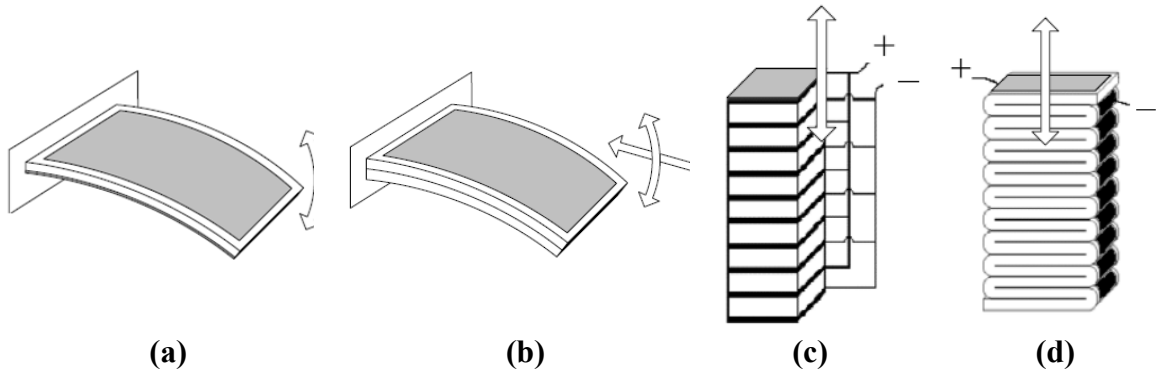

Figure 2-5: Some selected non pre-stretch DEAs: a) unimorph b) bimorph c) stack d) folded actuator adapted from [18].

2.6 Failure modes

This section presents three failure modes studied and investigated in [21].

2.6.1 Dielectric elastomer strength

When a dielectric breakdown occurs, sparks jump from one electrode to the other through the deflected region. At this point, the DEA fails and is no longer functioning. Dielectric breakdown mechanisms appear different for various materials [37]. The proposed elastomer failure criteria were experimentally tested for VHB 4905/4910 materials with different pre-stretch ratios [19]. The results showed that the breakdown field was inversely proportional to the thickness of the stretched elastomer, and it increased from 17 MV/m to 270 MV/m from no pre-strain to 36 times of its initial area. The explanation of this effect is based on elastomer molecular structure [23]. A typical elastomer is composed of long chains of monomer, cross-linked at points hundreds of monomers apart. When the elastomer is pre-stretched bi-axially, the chains form a grid that is perpendicular to the applied electric field. Therefore, these chains with high cross-section impede accelerating charges from gaining enough energy to start an electrical breakdown [19]. Figure 2-6 shows an electrical breakdown caused by a defective dielectric film.

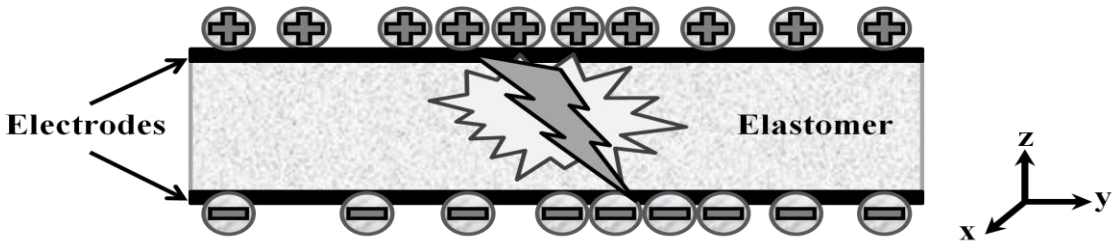

Figure 2-6: Schematic cross-section representation an electrical breakdown through a dielectric film deflected region adapted from [38] .

2.6.2 Pull-in instability

Typically, pull-in failure occurs when the Maxwell pressure becomes greater than the compressive stress of the elastomer. As a result, the film collapses into a complex 3D wrinkling patterns. The extreme local deformations caused by pull-in may have eventually caused either material or dielectric strength failure [38]. It has been suggested that pull-in failure is strongly affected by stretch rate.

3: Investigated Design

In this section, the actuator studied in this work is presented. In Lochmatter's thesis [18], an inflated spherical dielectric elastomer, hereafter called balloon-shape actuator (BSA), was proposed. The BSA consists of a thin walled spherical dielectric elastomer (DE) having two compliant electrodes on the internal and external surfaces. This actuator belongs to the pre-stretched DEAs category (see Section 2.5.1). To pre-stretch the elastomer, the balloon is inflated with incompressible fluid, air in this work. The advantage of this pre-stretching method is the simplicity of its structural support, which does not require the use of external equipment such as frames, clamps, or springs. When an electrical field is applied, an electrostatic pressure *P*, known as Maxwell pressure, is induced in the inner and outer surfaces of the actuator [13]. Due to the attraction of the opposing charges, the electrodes squeeze the elastomer in its radial thickness direction, resulting in a radial expansion of the BSA, as shown in Figure 3-1.

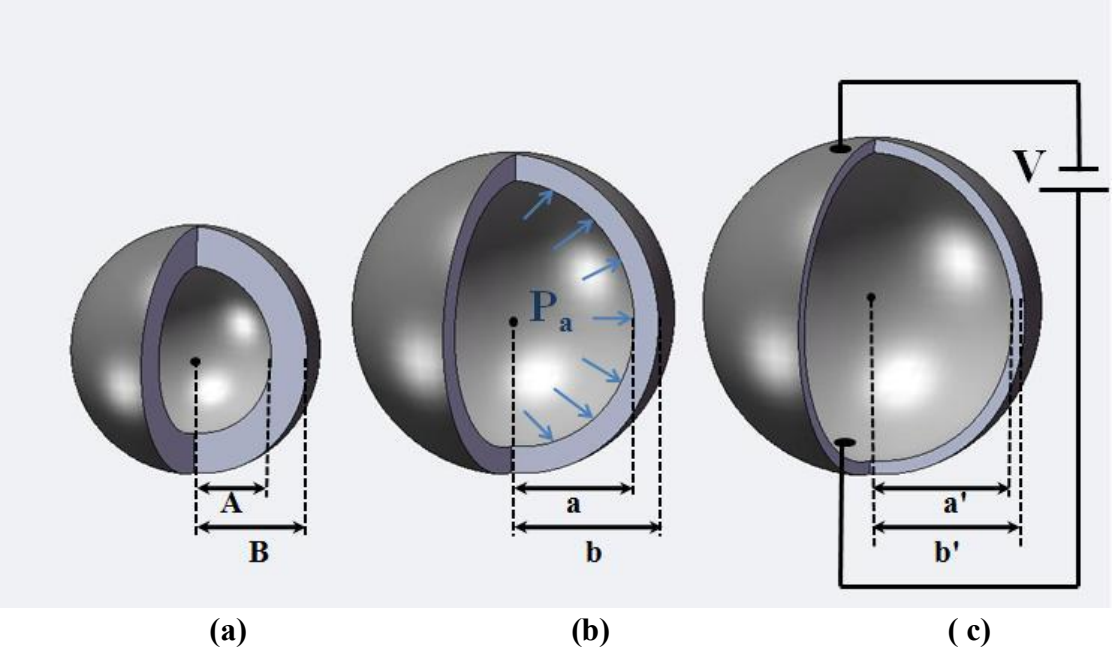

Figure 3-1: Schematic representation of a BSA: a) at rest b) inflated c) electrically activated.

A novel BSA actuation modality is proposed here. Besides exhibiting spherically symmetric radial expansion, the BSA could, in fact, potentially be used to move loads vertically as shown in Figure 3-2. Specifically, Figure 3-2-a shows an inflated BSA when no electrical field is applied; Figure 3-2-b shows the BSA compressed by a heavy load when no electrical field is applied; and Figure 3-2-c shows the BSA compressed by the same load used in Figure 3-2b–in this case, when an electrical field is also applied. By modulating the electrical field, the position of a heavy load can therefore be controlled.

The BSA radial deformation, which is schematically presented in Figure 3-1 and is hereafter referred as "Case study I", and the BSA lifting behaviour, which is schematically presented in Figure 3-2 and is referred as "Case study II" in the following sections, are investigated in detailed in this thesis.

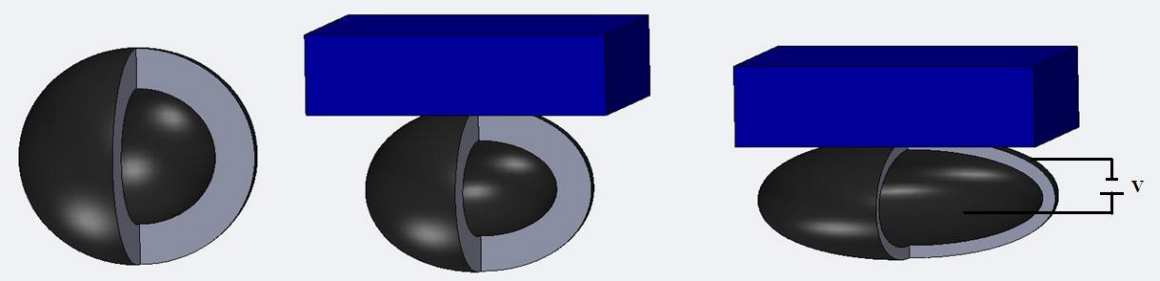

(a) **(b)** **(c)**

Figure 3-2: Schematic representation of the BSA activation under compressive load test procedure steps: a) inflated balloon; b) vertically compressed balloon; c) electrically actuated balloon.

4: Materials Characterizations and Planar DEA Modelling

4.1 Material Manufacturing of the BSA

A typical DEA consists of a thin layer of elastomer with compliant electrodes on both sides. A BSA has a spherical configuration consisting of a thin layer of a silicone elastomer with two compliant electrodes painted on the inner and outer surfaces of the elastomer. In the following section, the materials used in our work are introduced and their models discussed.

4.1.1 Elastomer Material

The material used as dielectric elastomer was TC-5005 (BJB,USA); this was also used by Carpi *et al.* in [39] and presented good overall performance. It is a soft silicone material that is commercially available as a three-component product: A, B and C. The curing component B was mixed with component A at a ratio of 1:10. Then component C was added at ratio of 50% to the total weight of TC-5005 A/B in order to increase the elongation and lower the amount of force needed to elongate the final elastomer. To obtain a homogenous mixture, it was placed in an ultrasonic shaker for 150 seconds. Then the solution was poured into an acrylic square with size 21 cm x 21 cm, and cured at room temperature for 24 hours to create a flat planer sample with a thickness of 1 mm.

4.1.2 Electrodes Material

One method of preparing electrodes consisted of using a silicone/carbon-black mixture. About 20 ml of trichloroethylene was used to dissolve 1 g of silicone mixture, CAF4,

(Rhodorsil, France). Later, 0.8 g of conductive carbon black powder, Vulcan xc72r (FBO, Brampton), was added to the mixture. This electrode material was applied on the DE elastomer with a fine brush.

4.2 Linear Modelling of the BSA elastomer material

Elastomers are capable of sustaining very high stretches. It is possible to derive the relation between the amount of applied force to stretch the elastomer and its extension. The derivation is illustrated by referring to a simple experiment in which a piece of elastomer was stretched while the corresponding force was measured. It should be noted that for simplifying the mathematical modelling of the material, time-independent models of DE were considered in the thesis.

The Young's Modulus, *Y*, of samples was obtained experimentally; tests were performed by using four dog-bone specimens as illustrated in Figure 4-1. Their specifications are provided in Table 4-1.

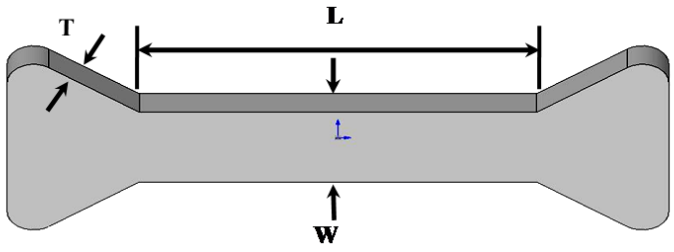

Figure 4-1: Schematic of the bone shaped sample used for measuring the Young's Modulus of TC-5005 silicone [40].

Table 4-1: Specifications of four different dog-bone shaped specimens [40].

Specimen #	Length(mm) L	Width(mm) W	Thickness(mm) T
1	23.00	4.82	2.38
2	23.7	3.93	2.97
3	24.83	4.21	3.09
4	25.87	5.04	2.43

An Instron Microtester (Model No. 5848) was used to perform the tests. A tensile load was applied at a constant rate until failure of the dog-bone specimen being tested was recorded. The force-displacement curves that are shown in Figure 4-2 present the results for the four different specimens.

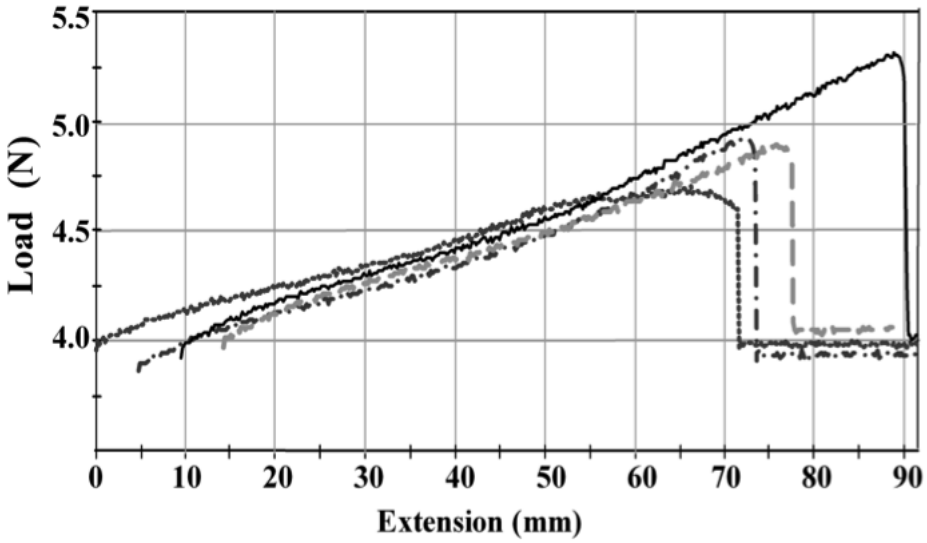

Figure 4-2: Experimental results used to measure the Young's Modulus of TC-5005 silicone [40].

The Young's Modulus of the different samples is provided in Table 4-2. The averaged Young's Modulus was 44.7 kPa. However, it is clear from Figure 4-2 that this elastomer

has non-linear mechanical behaviour. To study such behaviour, we repeated the experiment with the assumption of a hyper-elastic material model, as it will be discussed in the next section.

Table 4-2: Measured Young's Modulus for four specimens [40].

Specimen #	Tensile stress at Break(Standard) (MPa)	Load at Maximum Tensile extension (N)	Tensile stress at Maximum Tensile extension (MPa)	Modulus (Automatic Young's) (MPa)
1	0.34714	3.98550	0.34714	**0.03953**
2	0.34322	3.93437	0.34269	**0.04535**
3	0.35093	4.02898	0.35093	**0.04325**
4	0.35328	4.05258	0.35298	**0.05074**

4.3 Non-Linear Modelling of the BSA elastomer

Early analyses of DE used linear (Hookean) material models. However, studies have shown that for large deformation, a linear model is inadequate for predicting the nonlinear behaviour of DE material [19].

These issues can be addressed with hyper-elastic material models such as Neo-Hookean, Mooney-Rivlin, and Ogden. The mechanical behaviour of TC-5005 was experimentally determined through a tensile test by using Instron microtester. The initial dimensions of the tested sample were L= 9.1mm, W=3.04 mm, and T=2.18 mm. The test data were fitted with three non-linear models by using the fitting toolbox of commercial software, ANSYS; the fitting curves are presented in Figure 4-3 for the Neo-Hookean model, in Figure 4-4 for the Moony-Rivlin model, and in Figure 4-5 for the Ogden model. Figure 4-5 shows that the Ogden model is capable of fitting the observed behaviour in the entire range of measurements.

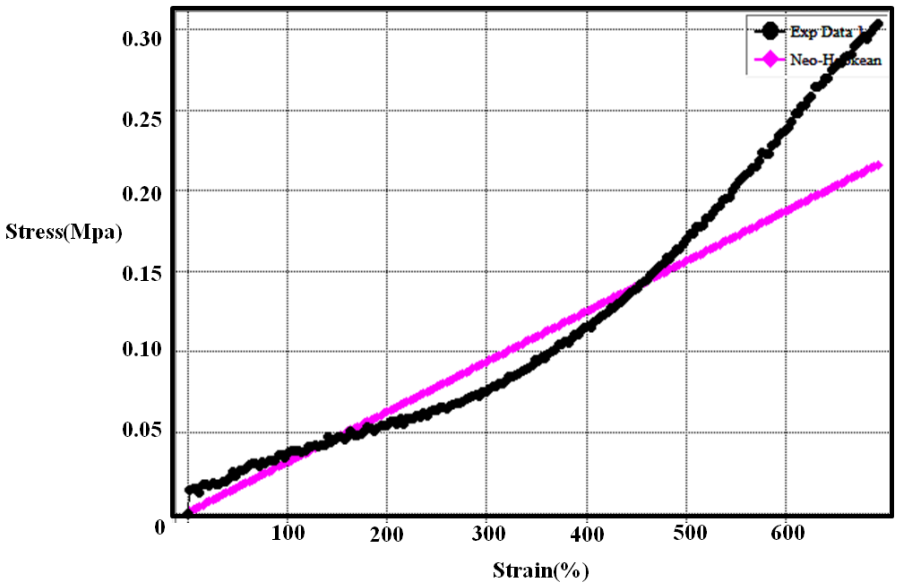

Figure 4-3: Stress-strain curve of TC-5005 elastomer material and fitting of the experimental data with hyperelastic Neo-Hookean model

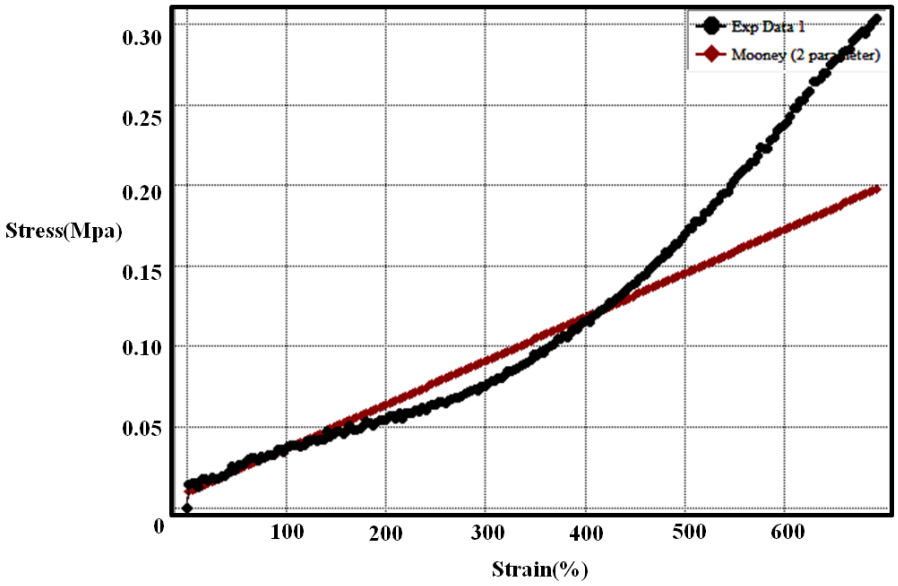

Figure 4-4: Stress-strain curve of TC-5005 elastomer material and fitting of the experimental data with hyperelastic Mooney-Rivlin model

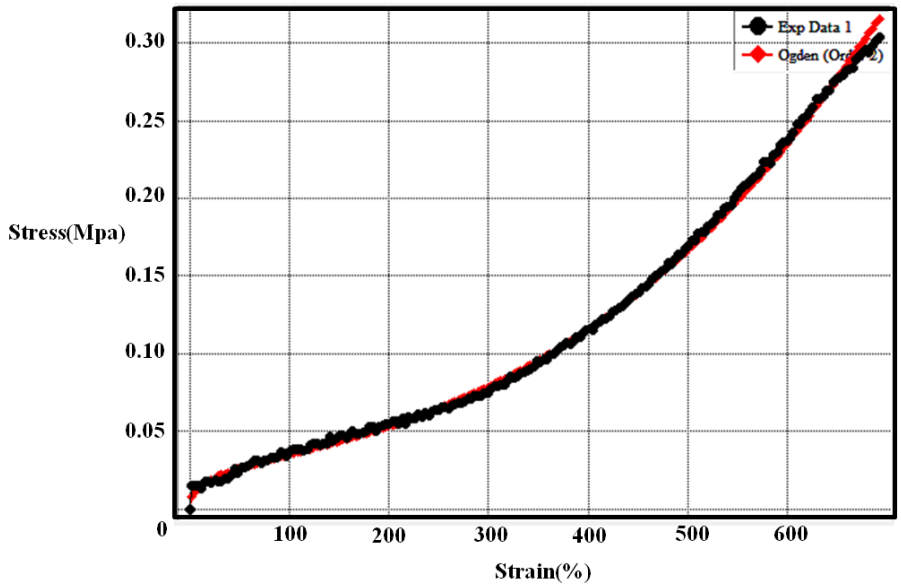

Figure 4-5: Stress-strain curve of TC-5005 elastomer material and fitting of the experimental data with hyperelastic Ogden model.

In this thesis, the BSA was radially deformed up to 200%. Since the Mooney-Rivlin model well predicted strains in the 0-2 range, this model was used in this work. Mooney-Rivlin was preferred to the Ogden model as it had a simpler analytical formulation.

4.4 Experimental characterization of a planar DEA

In this section, we present the results of experimental tests conducted to obtain fundamental characteristics of a simple planar DE actuator made of the same material used for manufacturing the BSA. The geometrical simplicity of planar DEAs allows a relatively simple manufacturing process. Thus, it is expected that fewer imperfections will be introduced during manufacturing, resulting in reliable actuators and accurate measurements. During these tests, three constant pre-loadings were applied to the sample, and the active displacement was measured as a function of the activation voltage. It was

hypothesized that the electrical activation of a pre-stretched planar DEA would simply yield a variation of the BSA stiffness [41].

4.4.1 Experimental Set up and Result

To identify the relationship between the electrical field and the DEA stiffness reduction, an experiment was performed as follows. A planar DEA sample was fabricated using the same BSA manufacturing procedure as that explained in section 4.1. The development of a simple model of the DEA required a simplified representation of the behaviour of the BSA. A flat sample with the thickness of 1 mm was prepared, and cut in a parallelepiped shape of 70 mm height and 40 mm width. Electrodes were prepared by smearing on the flat silicone a liquid solution obtained by mixing carbon black powder, silicone, and trichloroethylene (see section 4.1.2). The electrodes almost completely covered the two sides of the planar DEA; an uncoated edge of about 5 mm was left all around the actuator to prevent potential electrical discharges at the sample edges.

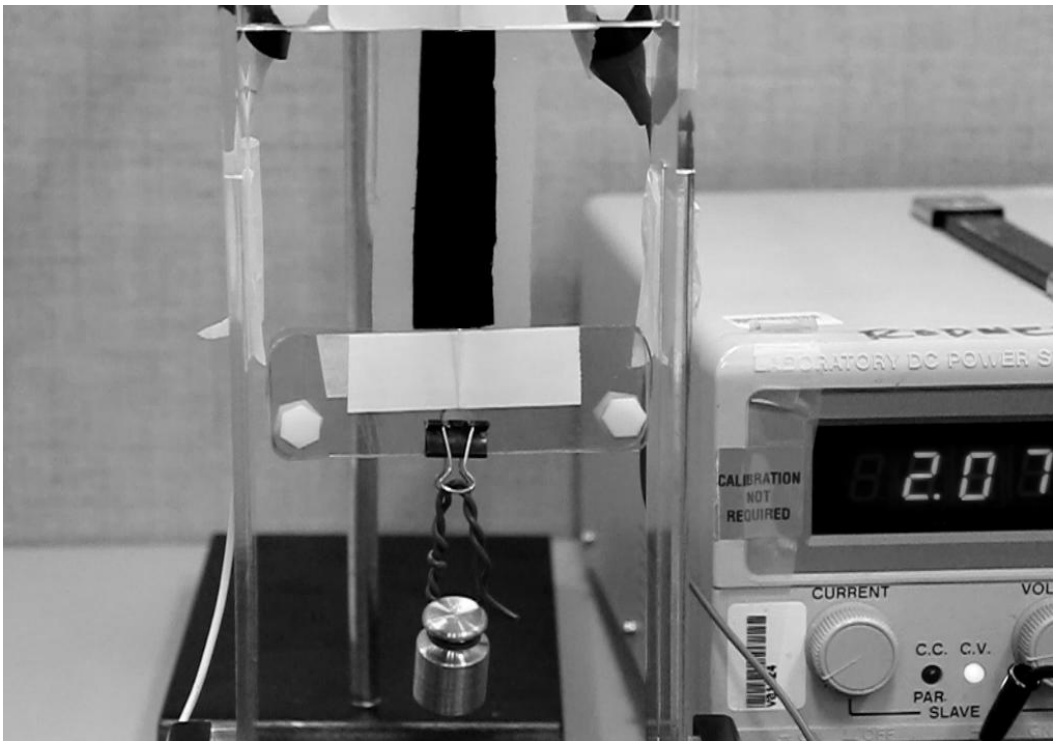

Figure 4-6: The bench test used for characterization of a planar DEA.

The planar DEA was positioned vertically, and clamped between two flat plates. The upper clamp was fixed, and the lower clamp with a weight of 20.11 g was left to move freely in the vertical position. The actuator was electrically activated by using a conventional power supply (GPC-1850D) connected to a high voltage converter (EMCO Q101-5). The displacements of the DEA were measured by taking pictures photographs with a high-resolution digital camera and post-processing the captured images with National Instrument Vision Builder (NIVB) software. The experiment was repeated by applying external weights of 10 g and 50 g to the lower clamp.

The post-processed results are presented in Figure 4-7. As shown, the strain, namely the ratio of total deformation $(\Delta L=L-L_0)$ to the initial length of actuator (L_0), increased

exponentially with the applied voltage. Furthermore, for larger loads, the strain grew faster with increasing voltage.

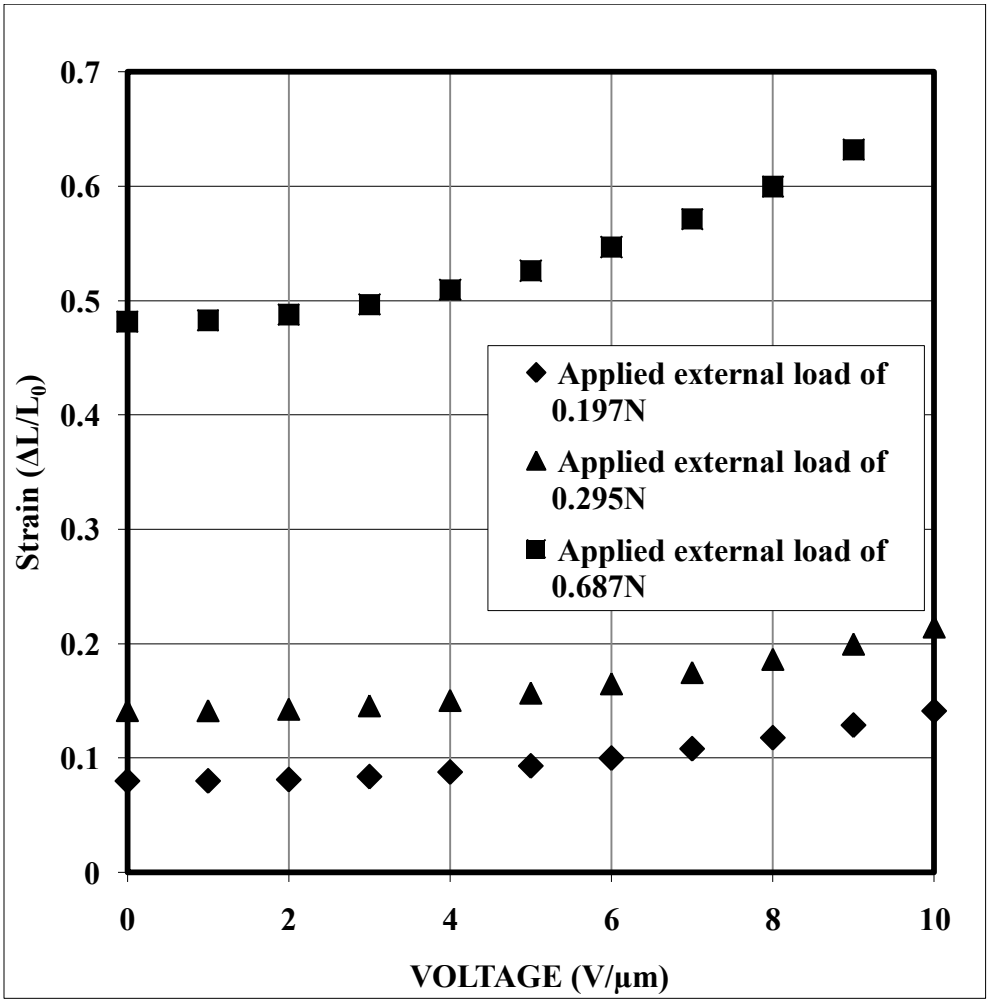

Figure 4-7: Strain vs. activation voltage under loading with 0.197 N, 0.295 N and 0.687 N.

Figure 4-8 shows reduction of the planar DEA stiffness obtained by increasing activation voltage under loading with 0.197 N, 0.295 N, and 0.687 N.

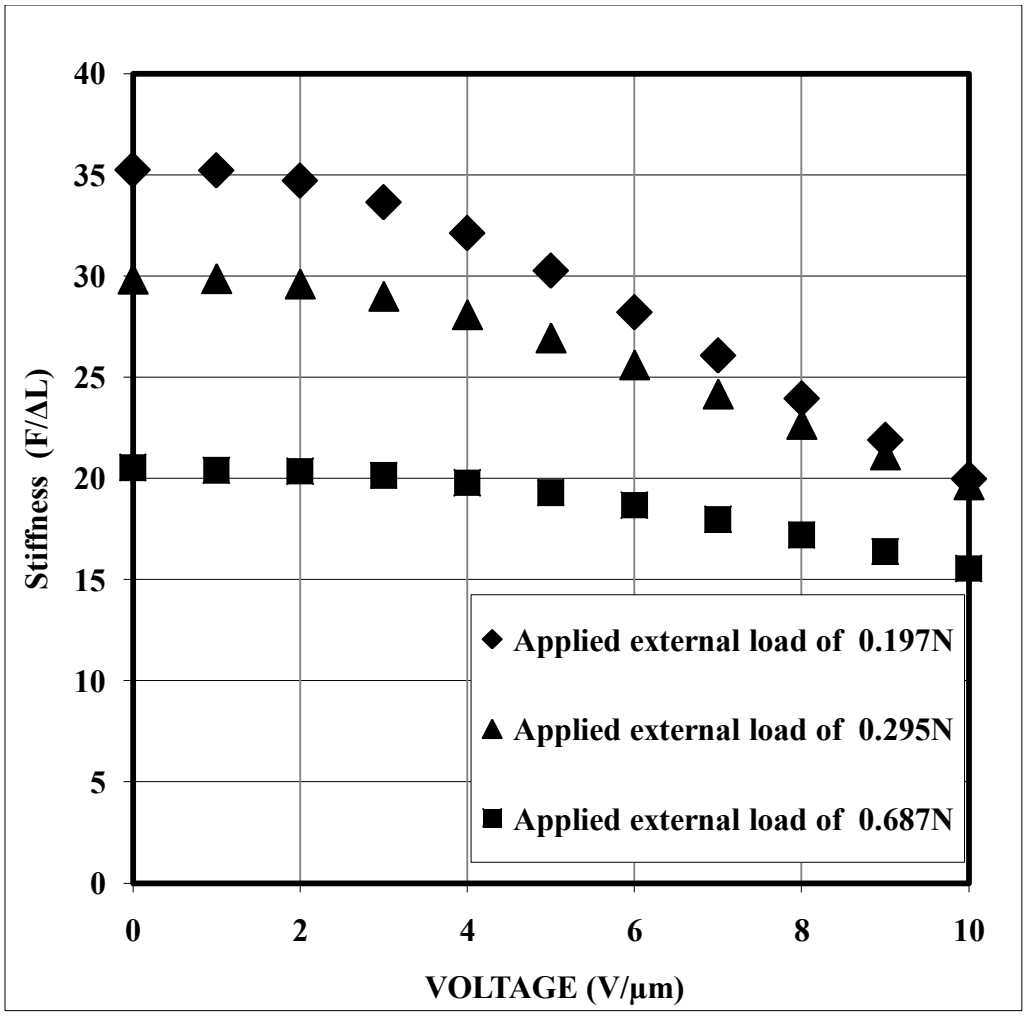

Figure 4-8: Stiffness vs. activation voltage under loading with 0.197 N, 0.295 N and 0.687 N.

5: Analytical Modelling of the BSA

In this chapter, the third objective of this thesis is addressed. The BSA radial deformation (Case study I) was analytically modelled. A non-linear hyperelastic model was used to estimate deformations exhibited by the actuator during inflation; a hyperelastic model was used since these deformations were large (>10%). A linear model was instead formulated to estimate deformations of the actuator when electrically activated because these deformations were small (<10%). The hyperelastic mechanical model was validated through an experimental procedure (see Section 7.1). The linear electromechanical model was instead validated by comparing analytical predictions with estimations obtained through FEM simulations (see Section 5.3); validating experimentally this electromechanical model would have required manufacturing an actuator perfectly spherical and without imperfections (see Section 6), which was beyond the proof-of-concept objective of this thesis.

It should be noted that the behaviour of the BSA under compressive loads (Case study II) was not analytically modelled in this thesis. In fact, variation of contact area and therefore of the constrains during BSA deformations makes the Case study II a very difficult problem to analyze analytically. It was therefore decided to defer the formulation of this analytical model to future studies fully focused to solve this specific mathematical problem.

5.1 Electrical modelling

The goal of the BSA electrical modelling is to derive an expression for the electrostatic pressure, *P*, exerted by the compliant electrodes, when a voltage, *V*, is applied between them. An inflated spherical actuator with inner radius *a*, and outer radius *b* is considered to be in its mechanical equilibrium before any electrostatic pressure is applied. The elastomeric BSA with spherical shape can be electrically modelled as a spherical capacitor. The electrical capacitance can be derived as [42] :

$$C = 4\pi\varepsilon \frac{ab}{b-a}\ , \tag{5.1}$$

where ε is dielectric permittivity which is constant since the elastomer is considered isotropic.

The stored electrostatic energy by the capacitor is [5]:

$$W_s = \frac{1}{2}CV^2 = 2\pi\varepsilon V^2 \frac{ab}{b\text{-}a}. \tag{5.2}$$

The electrostatic pressures P_a and $P_{b,}$ exerted by the internal and external electrodes, can be obtained by dividing the electrostatic force, *F*, over the area of the actuated electrodes as [5]:

$$P_a = \frac{F}{A} = \frac{F}{4\pi a^2} = \frac{|\nabla W_s|}{4\pi a^2}, \tag{5.3}$$

$$P_b = \frac{F}{A} = \frac{F}{4\pi b^2} = \frac{|\nabla W_s|}{4\pi b^2}. \tag{5.4}$$

F can be obtained as the gradient modulus of the stored electric energy, W_s, that is

$$|\nabla W_s| = \sqrt{\left(\frac{\partial W_s}{\partial a}\right)^2 + \left(\frac{\partial W_s}{\partial b}\right)^2} = 2\pi\varepsilon V^2 \frac{\sqrt{b^4 + a^4}}{(b-a)^2}. \tag{5.5}$$

The following equations present the applied pressures on the internal and external actuator surfaces due to the electrical activation of the BSA:

$$P_a = \varepsilon V^2 \frac{\sqrt{b^4 + a^4}}{2a^2(b-a)^2} \tag{5.6}$$

$$P_b = \varepsilon V^2 \frac{\sqrt{b^4 + a^4}}{2b^2(b-a)^2}. \tag{5.7}$$

5.2 Mechanical Modelling

A mechanical model is developed in three steps. In the first step, when no electrical field is applied, a large deformation analysis due to the inflation of the balloon is considered. It predicts the relation between inner pressure induced by compressed air and radial expansion of the sphere. In the next step, a small deformation analysis, considering

hypothesis of linear elasticity, serves to calculate the radial deformation due to electrostatic pressure when an electric field is applied to the electrodes of the actuator.

5.2.1 Inflation: Large Deformation Analysis Based on hyperelastic (non-linear) modelling

In this section, a non-linear model is derived for modelling the BSA large deformation. The following assumptions are considered; firstly, the elastomer is an isotropic, incompressible and hyper-elastic material. Secondly, we assume a spherical configuration for the BSA before and after inflation. Spherical coordinates are used to characterize the position of the material particles in undeformed position (R,Θ,Φ) and deformed (r, θ, φ) state. For a spherically symmetric expansion, the deformation is irrotational and the BSA only deforms radially as a function of its initial radius, $f(R)$:

$$r = f(R), \qquad \theta = \Theta, \qquad \phi = \Phi. \tag{5.8}$$

A hyperelastic or Green elastic material is a type of constitutive model for ideally elastic material for which the stress-strain relationship derives from a strain energy density function. The hyperelastic material is a special case of a Cauchy elastic material. Hyperelasticity provides a means of modellingthe stress-strain behaviour of elastomer materials. If G donates the gradient of the deformation, the Left Cauchy-Green tensor is [42]:

$$\mathrm{B} = GG^{\mathrm{T}} = \begin{bmatrix} B_{rr} & 0 & 0 \\ 0 & B_{\theta\theta} & 0 \\ 0 & 0 & B_{\phi\phi} \end{bmatrix} = \begin{bmatrix} \lambda_1^{\,2} & 0 & 0 \\ 0 & \lambda_2^{\,2} & 0 \\ 0 & 0 & \lambda_3^{\,2} \end{bmatrix} \tag{5.9}$$

where the principal stretches related to spherical coordinates are:

$$\lambda_1 = \lambda_r \qquad \lambda_2 = \lambda_\theta \qquad \lambda_3 = \lambda_\phi . \tag{5.10}$$

For an incompressible material, the following condition holds [43]:

$$\det G = \lambda_1 \lambda_2 \lambda_3 = 1. \tag{5.11}$$

Then,

$$(\lambda_r, \lambda_\theta, \lambda_\phi) = (\frac{1}{\lambda^2}, \lambda, \lambda), \tag{5.12}$$

where

$$\lambda = \lambda_\theta = \lambda_\phi = \frac{r}{R}. \tag{5.13}$$

By using the standard constitutive law, the Cauchy stresses, σ, can be determined as a function of a strain-energy density function, *W*, strain invariants *I1*, *I2*, and hydrostatic pressure part of stress [44]:

$$\sigma_{rr} = 2 \left[\frac{\partial W}{\partial I_1} + I_1 \frac{\partial W}{\partial I_2} \right] B_{rr} - \frac{I_1}{3} \frac{\partial W}{\partial I_1} - \frac{2I_2}{3} \frac{\partial W}{\partial \overline{I_2}} - \frac{\partial W}{\partial I_2} B_{rr}^{\,2} \Big] + \frac{p}{3}, \tag{5.14}$$

$$\sigma_{\theta\theta} = \sigma_{\phi\phi} = 2 \left[\left(\frac{\partial W}{\partial I_1} + I_1 \frac{\partial W}{\partial I_2} \right) B_{\theta\theta} - \left[\frac{I_1}{3} \frac{\partial W}{\partial \overline{I_1}} - \frac{2I_2}{3} \frac{\partial W}{\partial \overline{I_2}} - \frac{\partial W}{\partial I_2} B_{\theta\theta}^{\,2} \right] \right] + \frac{p}{3}, \tag{5.15}$$

where $\overline{I_1}$ and $\overline{I_2}$ are the first and the second invariants of the deviatoric component of the left Cauchy-Green deformation tensor, and for an incompressible material, they are equal to principal stretches [44]:

$$\overline{I_1} = I_1 = \lambda_1^2 + \lambda_2^2 + \lambda_3^2 = \frac{1}{\lambda^4} + 2\lambda^2, \tag{5.16}$$

$$\overline{I_2} = I_2 = \lambda_1^2 \lambda_2^2 + \lambda_2^2 \lambda_3^2 + \lambda_3^2 \lambda_1^2 = 2\frac{1}{\lambda^2} + \lambda^2. \tag{5.17}$$

As shown in section 4.3, Mooney_Rivlin model is suitable for this hyperelastic material with the following strain-energy density function, *W*, as [44]:

$$W = \frac{\mu_1}{2} \left(I_1 - 3 \right) + \frac{\mu_2}{2} \left(I_2 - 3 \right) \tag{5.18}$$

Substituting equations (5.16) to (5.18) in equations (5.14) and (5.15) leads to the following Cauchy stress equations:

$$\sigma_{rr} = \frac{2}{3}(\mu_1 + \mu_2\lambda^2)(\frac{1}{\lambda^4} - \lambda^2) + p \tag{5.19}$$

$$\sigma_{\theta\theta} = \sigma_{\phi\phi} = \frac{1}{3}(\mu_1 + \mu_2\lambda^2)(\frac{1}{\lambda^4} - \lambda^2) + p. \tag{5.20}$$

Substituting above stresses into bellow equilibrium equation [44],

$$\frac{d\sigma_{rr}}{dr} + \frac{1}{r}(2\sigma_{rr} - \sigma_{\theta\theta} - \sigma_{\phi\phi}) = 0, \tag{5.21}$$

forms the following differential equation :

$$\frac{d\sigma_{rr}}{dr} + \frac{2}{r}(\mu_1 + \mu_2\lambda^2)(\frac{1}{\lambda^4} - \lambda^2) = 0. \tag{5.22}$$

Equation (5.22) can be integrated with respect to radius using the following obtained equation:

$$\frac{dr}{r} = \frac{\lambda}{1 - \lambda^3} d\lambda \tag{5.23}$$

which is simplified to:

$$\sigma_{rr} = \mu_1\left((\frac{2}{\lambda} + \frac{1}{2\lambda^4})\right) + \mu_2\left((\frac{1}{\lambda^2} - 2\lambda)\right) + C. \tag{5.24}$$

If the sphere which has inner radius of A and outer radius of B, is subjected to inner pressure P_a and outer pressure P_b , then after deformation, the inner radius and outer radius are;

$$f(A) = a \qquad f(B) = b \tag{5.25}$$

Applying boundary conditions σ_{rr}= -P_a on inner surface and σ_{rr}= -$P_b$on the outer surface yields:

$$-P_a = \mu_1\left((\frac{2}{\alpha} + \frac{1}{2\alpha^4})\right) + \mu_2\left((\frac{1}{\alpha^2} - 2\alpha)\right) \tag{5.26}$$

$$-P_b = \mu_1\left((\frac{2}{\beta} + \frac{1}{2\beta^4})\right) + \mu_2\left((\frac{1}{\beta^2} - 2\beta)\right) \tag{5.27}$$

where α=a/A, and β=b/B.

Solving these equations gives the relation between pressure and deformation of the BSA as:

$$P_a - P_b = \left[[2\left((\frac{1}{\beta} - \frac{1}{\alpha})\right) + \frac{1}{2}\left((\frac{1}{\beta^4} - \frac{1}{\alpha^4}) - \frac{2\mu_2}{\mu_1}(\beta - \alpha) + \frac{\mu_2}{\mu_1}\left((\frac{1}{\beta^2} - \frac{1}{\alpha^2})\right)\right]\mu_1\right) \tag{5.28}$$

5.2.2 Electrical activation: Small Deformation Analysis based on Linear Modelling

In order to derive the strains and stresses produced by two exerted pressures P_a and P_b on the internal and external BSA surfaces, a mechanical analysis of the actuator was carried

out when it was electrically activated. Because the deformation of the BSA under the applied electric field is very small, we model the actuator as a linear elastic body.

Carpi [5] [39] mechanically modelled a cylindrical DEA by using the Navier's equations to determine the relations between applied 'Maxwell pressure and corresponding actuator deformations, considering linearly elastic homogenous isotropic materials. For linearly modelling of the BSA, we can consider Navier's equations for an isotropic and homogenous dielectic elastomer material in spherical coordinates [45]. Assuming time-invariant displacements and in the absence of body forces per unit mass (such as gravity); the Navier's equations are simplified to:

$$(\lambda+\mu)\frac{\partial}{\partial r}\left(\frac{1}{r^2}\frac{\partial}{\partial r}(r^2u_r)+\frac{1}{r\sin\theta}\frac{\partial}{\partial\theta}(u_\theta\sin\theta)+\frac{1}{r\sin\theta}\frac{\partial u_\phi}{\partial\phi}\right) \\ +\mu\left(\nabla^2u_r-\frac{2}{r^2}u_r-\frac{2}{r^2}\frac{\partial u_\theta}{\partial\theta}+\frac{2u_\theta\cot\theta}{r^2}-\frac{2}{r^2\sin\theta}\frac{\partial u_\phi}{\partial\phi}\right)=0, \tag{5.29}$$

$$(\lambda+\mu)\frac{1}{r}\frac{\partial}{\partial\theta}\left(\frac{1}{r^2}\frac{\partial}{\partial r}(r^2u_r)+\frac{1}{r\sin\theta}\frac{\partial}{\partial\theta}(u_\theta\sin\theta)+\frac{1}{r\sin\theta}\frac{\partial u_\phi}{\partial\phi}\right) \\ +\mu\left(\nabla^2u_\theta+\frac{2}{r^2}\frac{\partial u_r}{\partial\theta}-\frac{u_\theta}{r^2\sin^2\theta}-\frac{2\cos\theta}{r^2\sin^2\theta}\frac{\partial u_\phi}{\partial\phi}\right)=0, \tag{5.30}$$

$$(\lambda+\mu)\frac{1}{r\sin\theta}\frac{\partial}{\partial\phi}\left(\frac{1}{r^2}\frac{\partial}{\partial r}(r^2u_r)+\frac{1}{r\sin\theta}\frac{\partial}{\partial\theta}(u_\theta\sin\theta)+\frac{1}{r\sin\theta}\frac{\partial u_\phi}{\partial\phi}\right) \\ +\mu\left(\nabla^2u_\phi-\frac{1}{r^2\sin^2\theta}u_\phi+\frac{2}{r^2\sin\theta}\frac{\partial u_r}{\partial\phi}+\frac{2\cos\theta}{r^2\sin^2\theta}\frac{\partial u_\theta}{\partial\phi}\right)=0. \tag{5.31}$$

In these equations, μ and λ are Lamè's constants, and u_r , u_θ and u_φ are displacements along spherical coordinates, r, θ, and φ. Reasonably assuming the BSA does not displace in θ and φ direction when it is activated, the radial displacements u_r depends only on coordinated r as:

$$u_\theta = 0, \tag{5.32}$$

$$u_r = u_r(r), \tag{5.33}$$

$$u_\phi = 0. \tag{5.34}$$

With these assumptions, equations (5.30) and (5.31) are null and equation (5.29) become:

$$\frac{d}{dr}\left(\frac{1}{r^2}\frac{d}{dr}(r^2 u_r)\right) = 0. \tag{5.35}$$

Solving equation (5.35) yields to:

$$u_r = \frac{c_1}{3} r + \frac{1}{r^2} c_2, \tag{5.36}$$

where c_1 and c_2 are arbitrary constants.

According to the relation between strains (S_{rr}, $S_{\theta\theta}$, and $S_{\varphi\varphi}$) and displacements in Spherical Coordinates and considering equation (5.36), strains are:

$$S_{rr} = \frac{du_r}{dr} = \frac{c_1}{3} - \frac{2}{r^3} c_2 \tag{5.37}$$

$$S_{\theta\theta} = \frac{u_r}{r} + \frac{1}{r}\frac{du_\theta}{d\theta} = \frac{u_r}{r} = \frac{c_1}{3} + \frac{1}{r^3} c_2 \tag{5.38}$$

$$S_{\phi\phi} = \frac{1}{r\sin\theta}\frac{du}{d\phi} + \frac{u_r + u_\theta \cot\theta}{r} = \frac{u_r}{r} = \frac{c_1}{3} + \frac{1}{r^3} c_2. \tag{5.39}$$

Strains and stresses (σ_{rr}, $\sigma_{\theta\theta}$, and σ_{zz}) are related by means of the material constitutive equations, represented here by the Hooke's law, since the linear elasticity is assumed for small deformation of the BSA elastomer due to the electrical activation [46]. Here the general form of strains and stress can be expressed in terms of Lam`e's constants , λ and μ ,as follows [46]:

$$\sigma_{rr} = \lambda(S_{rr} + S_{\theta\theta} + S_{\phi\phi}) + 2\mu S_{rr} = \frac{2}{3}(\lambda + \mu)c_1 - \frac{1}{r^3}(\lambda + 4\mu)c_2 \tag{5.40}$$

$$\sigma_{\theta\theta} = \lambda(S_{rr} + S_{\theta\theta} + S_{\phi\phi}) + 2\mu S_{\theta\theta} = (\lambda + \frac{2}{3}\mu)c_1 + \frac{2}{3}\mu c_2 \tag{5.41}$$

$$\sigma_{\phi\phi} = \lambda(S_{rr} + S_{\theta\theta} + S_{\phi\phi}) + 2\mu S_{\phi\phi} = (\lambda + \frac{2}{3}\mu)c_1 + \frac{2}{3}\mu c_2. \tag{5.42}$$

The unknown constants, c_1 and c_2 , can be obtained by imposing the following boundary conditions for the stresses:

$$\sigma_{rr}\big|_{r=a} = -p_a, \tag{5.43}$$

$$\sigma_{rr}\big|_{r=b} = -p_b, \tag{5.44}$$

while the Maxwell pressure, *P,* is compressive, the stresses are considered to be negative. So,

$$(\lambda + \frac{2\mu}{3})c_1 - \frac{4\mu}{a^3}c_2 = -p_a \tag{5.45}$$

$$(\lambda + \frac{2\mu}{3})c_1 - \frac{4\mu}{b^3}c_2 = -p_b. \tag{5.46}$$

These equations can be solved to find the unknowns c_1 and c_2 as:

$$c_1 = \frac{-a^3 p_a + b^3 p_b}{(a^3 - b^3)(\lambda + \frac{2\mu}{3})}, \tag{5.47}$$

$$c_2 = \frac{a^3 b^3 (p_b - p_a)}{4\mu(a^3 - b^3)}. \tag{5.48}$$

Therefore, by substituting c_1 and c_2 in (5.36) the radial displacement of inner and outer radii of the BSA due to the induced Maxwell pressure on the inner and outer surfaces of the actuator can be predicted as:

$$\frac{\Delta a}{a}\Big|_{active} = \frac{3}{4}\frac{b^3(p_b - p_a)}{Y(a^3 - b^3)} \tag{5.49}$$

$$\frac{\Delta b}{b}\Big|_{active} = \frac{3}{4}\frac{a^3(p_b - p_a)}{Y(a^3 - b^3)}. \tag{5.50}$$

5.3 Electrical Activation: Validation based on Finite Element Method (FEM) Modelling

To validate the analytical model obtained for passive deformation in section 5.2.2, finite element simulations were carried out. We used ANSYS11 for the finite element modelling of the hemisphere to calculate the amount of deformation for the given Maxwell pressure. This pressure was calculated analytically based on the applied voltage for an isotropic linear elastic material, and was applied to the inner and outer surfaces of the modelled half BSA. Specifications of the simulated BSA are given in Table 5-1. The meshing of the model was done with BRICK45 element type (see Figure 5-1).

Table 5-1: BSA specifications for FEM modelling

Parameter	Parameter value
Inner radius, a	0.029065 (m)
Outer radius, b	0.030065 (m)
Poisson's ratio, υ	0.499
Young's Modulus Y	44700 (Pa)
Dielectric constant ε	5

Maxwell pressure for different voltages was calculated analytically using equations (5.6) and (5.7), and it was applied to the created BSA. The deformation of the external radius of the simulated BSA, Δb, is compared with the analytical passive deformation provided by equation 5.64.

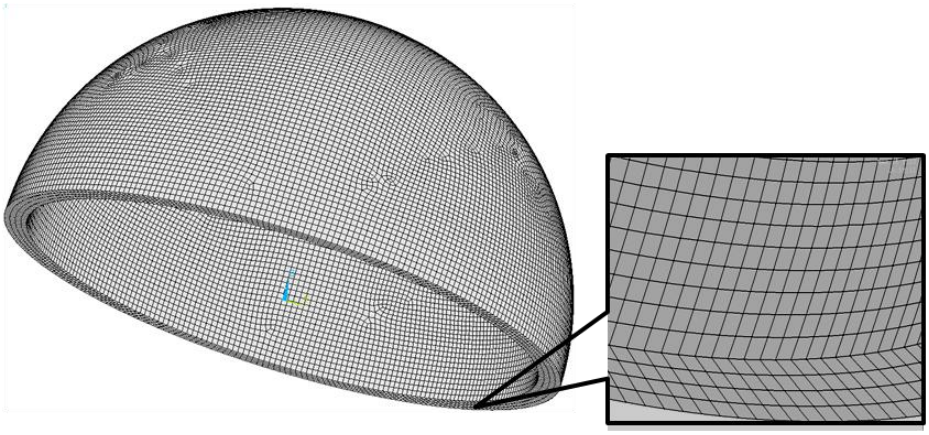

Figure 5-1: FEM model of hemisphere actuator in ANSYS.

In Figure 5-2, strain percentage is plotted as a function of applied voltage for the analytical and FEM model. As shown in the figure, the results match with 0.03% error.

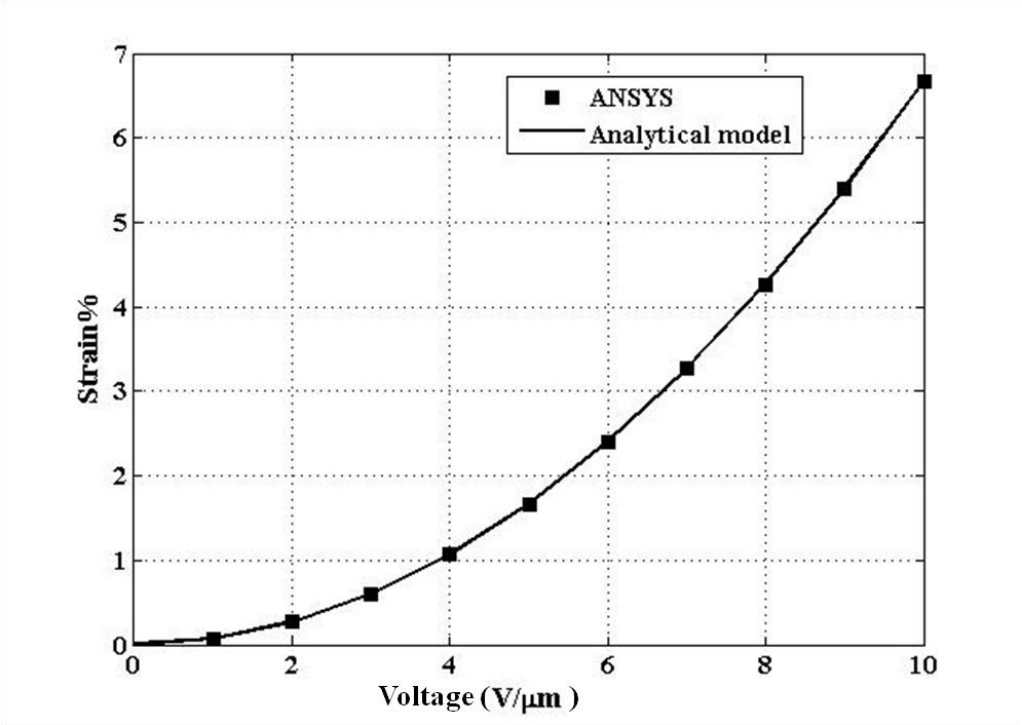

Figure 5-2: Strain (Δb/B)% versus applied voltage.

6: Manufacturing of the BSA

In this chapter, two different BSA manufacturing procedures are proposed to fulfil the forth objective of the thesis.

In the first manufacturing procedure, a moulding technique is proposed to fabricate the BSA. Such a technique allows fabricating spherical actuators. In order to limit the cost, moulds were fabricated by using a rapid-prototyping manufacturing machine. Surface was therefore not very smooth and thicknesses of the prototypes were not very uniform. While this procedure was shown to be feasible and enabled testing the hyperelastic model used to predict deformation during inflation, it was not adequate for quantitative tests needed to investigate the Case study II. A second simplified manufacturing procedure was therefore developed, as discussed in the following paragraphs.

6.1 Moulding technique for spherical prototypes

A plastic mould was developed to obtain a BSA with an almost homogenous spherical shape. This spherical mould consists of one inner sphere and four outer sphere parts that were designed with a CAD software (SolidWorks). We used a 3D printer to create the plastic physical mould from a three-dimensional CAD model. The printer used CAD data to drive an inkjet-type print-head to deposit a hot liquid ABS plastic filament in thin-layer increments in the XY plane, building up the mould in the Z-axis direction. Figure 6-1 shows the schematic representation of CAD design for the five different parts of the plastic mould. Figure 6-2 shows a picture of our designed plastic mould for manufacturing of the BSA. Elastomer material of the BSA, explained in section 4.1.1,

was prepared and poured into the mould, and then placed inside a vacuum chamber for half an hour to remove the air bubbles trapped in the polymer.

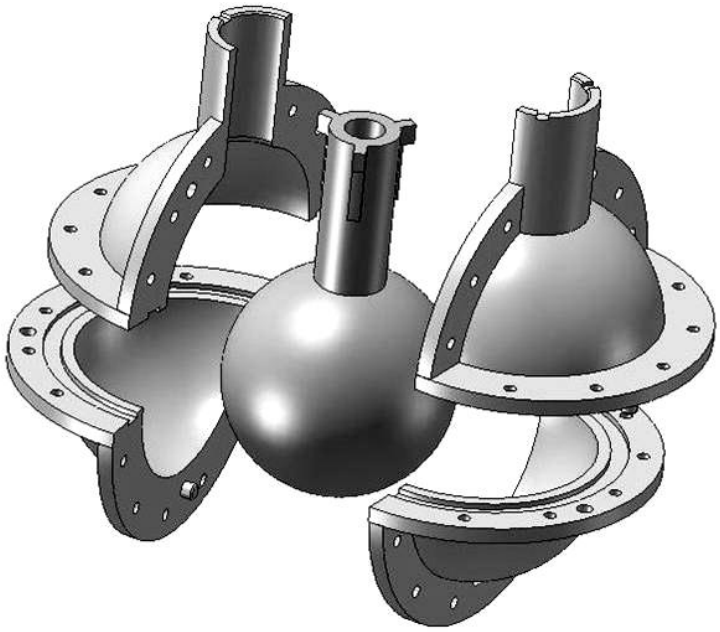

Figure 6-1: Schematic representation of the spherical mould.

The sample was then cured at room temperature to form a spherical elastomer with an inner radius of 30 mm and a thickness of 1 mm. One electrode was painted on the inner surface of the prepared sample and one on the outer surface, as explained in section 4.1.2. Finally, the prototype was inflated with air to introduce a uniformly distributed pressure perpendicular to the inner surface of the polymer, causing radial pre-strain in the actuator. Experiments showed that by using this manufacturing procedure, a spherically symmetric BSA could be manufactured for use in performing inflation tests and validating the nonlinear mechanical analytical model that was developed.

It should be noted that the BSA wall thickness was not very uniform and it had variation of about ± 50µm. Therefore, the defective surface prevented us from electrically activating the developed prototype (thickness variation and surface defects cause electrical breakdown).

Figure 6-2: The used spherical mould for BSA manufacturing.

This issue could have been solved by using metallic moulds instead of plastic. However, metallic moulds were not fabricated because their extremely high cost did not justify the proof-of-concept tests required for this thesis. A second simplified procedure was therefore implemented to perform electromechanical tests, and is discussed in the next section.

6.1.1 Simplified manufacturing technique for validating the Case study II

A simplified and inexpensive manufacturing technique was developed to validate the fabrication feasibility and potential performance of balloon-shape actuators capable to

work in compressive mode (Case study II). We fabricated the BSA by pressurizing a DE cylindrical tube manufactured as follows. After preparation of flat elastomenrs manufactured as explained in section 4.1.1, they were cut in rectangular shapes to form flat elements weighing about 22 ± 5 g. Then two sides of each rectangular element were bonded by using 732 Multi-Purpose Sealant (Dow Corning Co., USA) to obtain a cylindrical shape. Electrodes, consisting of a silicone/carbon-black mixture (see section 4.1.2), were painted with a fine brush on the inner and outer surfaces of the elastomer tube. The product of each step explained above is shown in figure 6-3.

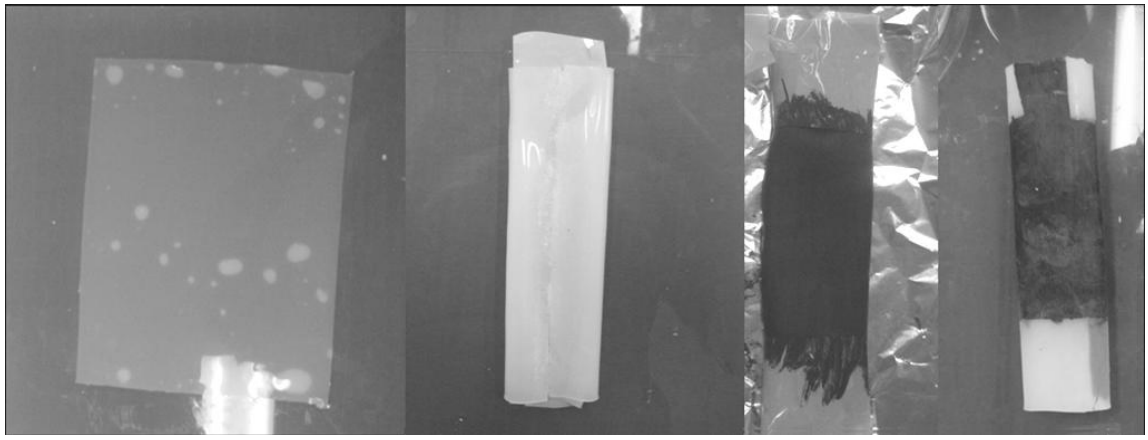

Figure 6-3: Manufacturing steps for simplified design of BSA: a) flat DE sample, b) cylindrical DE by bonding the edges of the flat sample) painted electrodes d) cylindrical DEA.

The tube was inflated with compressed air until a balloon-shape configuration was obtained; pressurization allowed radially pre-straining of the actuator. The compressed air introduced a uniformly distributed pressure perpendicular to the inner surface of the polymer, facilitating radial expansion of the balloon when electrically actuated. The advantage of this method of fabrication is that it is relatively simple and can be applied

easily. However, experiments have shown that if the edges were not bonded properly, then electrical break down would occur, resulting in actuator failure. Moreover, obtaining a spherical configuration from a cylindrical tube does not provide a perfectly symmetrically spherical shape. On the other hand, this process is simple and inexpensive and allows electrical activation of the fabricated prototypes. Therefore, we prepared BSAs using this method for running experiments to study BSA actuation under a compressive load (Case study II), where imperfect spherical configuration was not of concern.

6.2 Undesired BSA Features

Features that primarily caused failure of the BSA during the fabrication process are as follows:

- Non-uniform BAS thickness in fabrication process caused by misalignment of the mould, resulting in non-symmetrical deformation under actuation.

- Elastomer imperfection due to trapped bubbles, causing dielectric break down. Figure 6-4 depicts an example of a fabricated BSA with trapped bubbles in the elastomer.

- Small cracks in elastomer film that cause tearing in the actuator because of the pre-straining procedure that enlarges the crack area.

- Exceeding the maximum voltage. It has been observed during experiments that if the activating voltage exceeds 10 V/μm, electrical breakdown and actuator failure occur.

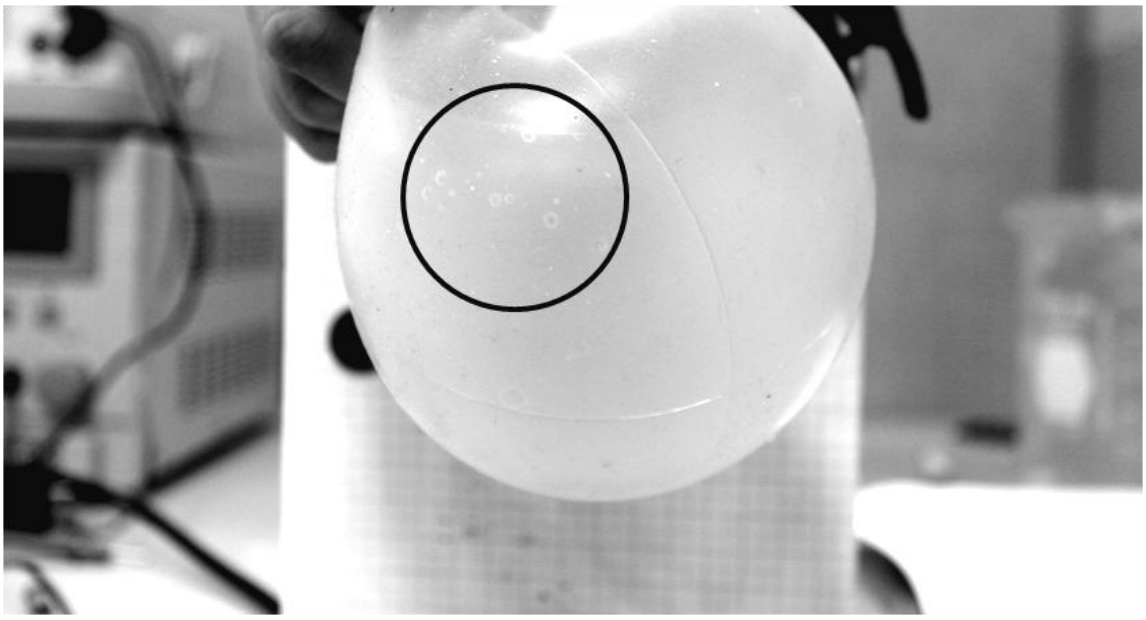

Figure 6-4: Trapped Bubbles in the BSA elastomer.

7: Experimental Results

Experiments were performed for validating the two case studies and thus fulfilling the fifth objective of this thesis. For the first case study, an experiment was run to obtain the relationship between the pressure inside the expanding balloon and its radial deformation. The experimental results were compared with the radial deformation of the expanding BSA predicted with both linear and non-linear analytical models. For the second case study, experiments were performed to determine the relation between radial deformation and applied load.

7.1 Experimental Validation of the Mechanical Modelling (Case study I)

A test was performed to compare the non-linear and linear analytical models presented in sections 5.2.1 and 5.2.2. A BSA sample with outer radius *B* equal to 30.65 mm and thickness equal to 1 mm was manufactured by using the spherical mould (see section 5.2.1 for details about the fabrication procedure). The pressure inside the BSA was measured with a pressure sensor (a Silicon on Sapphire Pressure Transmitter PX 4200-010 GI, Omega, USA) having a range of 0-10 psig. This pressure gauge was equipped with a plug-on display with single set-point, PM 1001 (Omega, USA), which constantly monitored the inside pressure. The other end of the pressure sensor was connected to a pressurised air-line. The BSA was inflated gradually, and the changes in diameter were measured by an imaging technique. Imaging post-processing software (Vision Builder Software, National Instruments) was used to detect diameter variations of the balloon

from the photographs taken by a high-resolution camera. Figure 7-1 shows two captured images of BSA before and after being inflated.

`

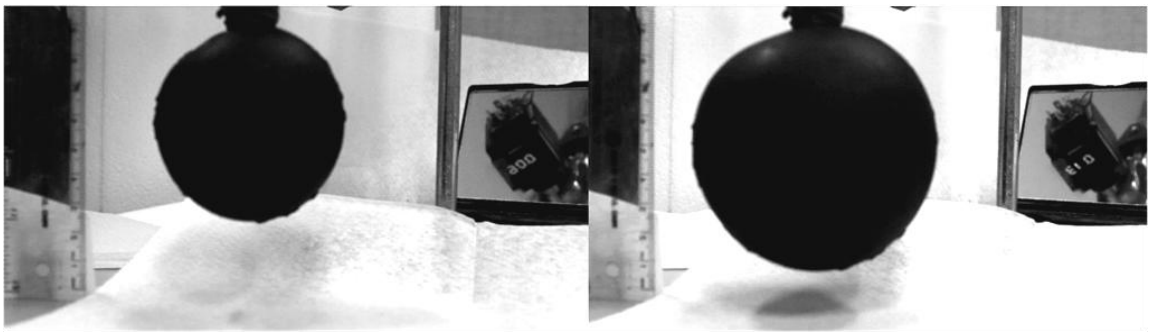

(a) **(b)**

Figure 7-1: Experimental set up for measuring the relationship between internal pressure and radius of the actuator when the actuator is gradually inflated but not activated, to validate the obtained mechanical modelling with experimental data. Snapshots of the experiments are presented in figures (a) and (b).

The results obtained from this test were fitted to the analytical result obtained by equation (5.28) and (5.62) for large and passive deformation modelling, as shown in Figure 7-2. Specifically, , p is the difference between the internal and external (atmospheric) pressures (P_{in}-P_{out} acting on the balloon-shape actuator), μ is the shear modulus of the polymer, H is its thickness, and λ is the ratio between the external radius of the balloon when it is inflated, b, and when it is in its initial condition, B. It can be seen that the non-linear analytical model fits better with the experimental results rather than the linear model. The error between the experimentally measured $Q_{experimental}$ and analytically predicted $Q_{analytical}$ was computed as:

$$error\% = 100\left|\frac{Q_{experimental} - Q_{analytical}}{Q_{analytical}}\right|, \tag{7.1}$$

where $Q = \frac{Pb}{\mu H}$.

The average error of 17.5% was calculated for nonlinear modelling.

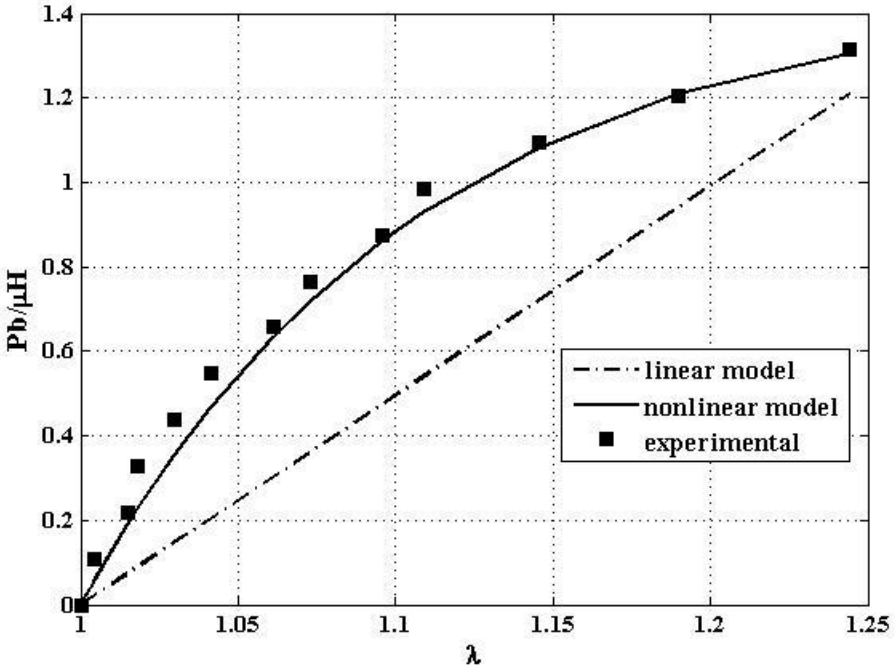

Figure 7-2: Relationship between internal pressure and stretch ratio (λ=b/B) of the balloon-shape actuator : Points are the experimental data that were fitted acceptable with the analytical model

7.2 BSA Activation under Compressive Load Experiments (Case study II)

For this case study, we carried out experiments to predict the relation between the inner pressure of a cylindrical BSA and its external radius for different applied voltages. Furthermore, radial deformation of the activated BSA was determined for different applied compressive loads, by an indirect measuring procedure.

7.2.1 Radial expansion due to internal pressure of the activated BSA for different applied voltages

Experiments were performed to determine the relation between the inner pressure of the balloon and its external radius, *b*, for various voltage differences applied to the actuator's electrodes. The tube actuator, whose manufacturing procedure was explained in section 6.1.1 , was connected to a pressurised air line at one side. The pressure inside the actuator was constantly measured using the pressure sensor mentioned in the previous section, which was fixed to the other side of the cylinder (see Figure 7-3-a). The changes in radius were measured by the imaging technique explained in section 7.1–the balloon was inflated gradually (Figure 7-3-b) and at 2-second intervals a photograph was taken with a high-resolution camera. The results obtained from this test are shown in Figure 7-4.

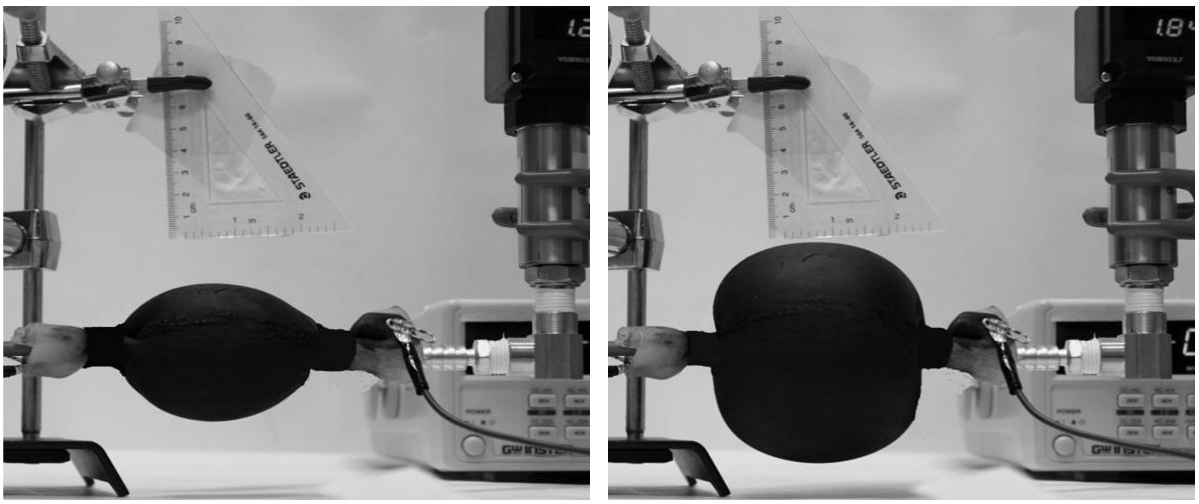

a) **b)**

Figure 7-3: Experimental set up for measuring the relationship between internal pressure and radius of the actuator for different applied voltages. Snapshots of the experiments are presented in figures a) and b).

Figure 7-4 shows the relationship between the internal and external (atmospheric) pressure difference and radius of the balloon-shape actuator for different values of the applied voltage, *V*. Note that in the initial condition, a small internal pressure (112660 Pa) was used to avoid the balloon collapsing on itself.

Figure 7-4 shows four curves obtained for four voltage differences. It should be noted that these experimental results do not represent an ideal scenario, because the tested BSA was manufactured starting from a cylindrical polymer, as explained in section 6.1.1, and both the flexible tubes used to pressurize the balloon and the wires connecting the electrodes of the balloon to the power supply obstructed slightly the longitudinal expansion of the actuator (Figure 7-3). Nonetheless, Figure 7-4 presents relevant experimental results as the relationship between voltage and pressure can be inferred.

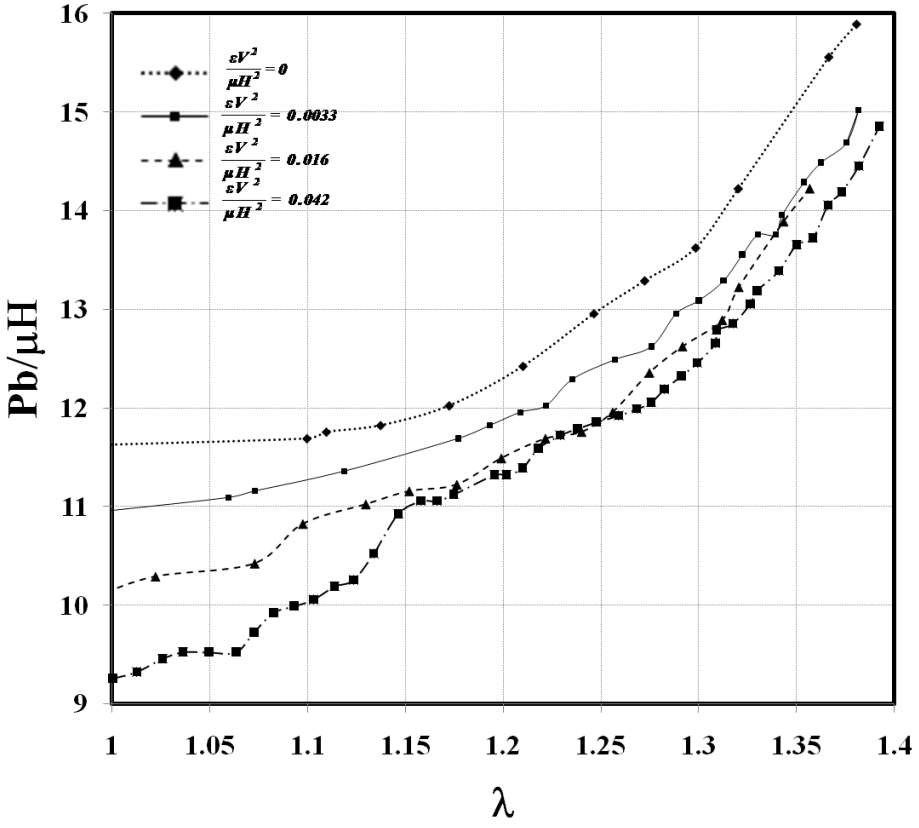

Figure 7-4: Relationship between internal pressure and radius of the balloon-shape actuator for different values of the applied voltage.

7.2.2 Force measurements

The main hypothesis of the case study II is that balloon-shape actuators can display large deformations under high compression loads. Given the specific features of our Instron Microtester, instead of performing a direct measurement of the deformation under different loading conditions we measured the variation of the force exerted by the actuator for fixed displacements imposed on the actuator by the Instron Microtester, and we subsequently derived the relationship between force and deformation, as explained in the next paragraph.

The experimental arrangement is shown schematically in Figure 7-5. Each balloon-shape actuator was separately placed between two non-conductive horizontal flat surfaces, as depicted in blue in Figure 7-5-a. The balloon was subsequently compressed until a defined distance between the flat surfaces (X2 in Figure 7-5-b) was reached; this distance was kept constant during the following phases of the test, namely X3=X2 (see Figure 7-5-b and Figure 7-5-c). By applying a high voltage difference between the electrodes, the thickness of the polymer was reduced. As a result, the volume inside the balloon consequently increased (see Figure 7-5-c), and therefore the pressure inside the balloon decreased. As a consequence of this pressure drop, the force exerted by the balloon on the two horizontal flat surfaces decreased, namely F3 < F2 (Figure 7-5-c). It should be remarked that the tests were performed at different fixed distances between the two non-conductive horizontal flat surfaces, namely X3=X2.

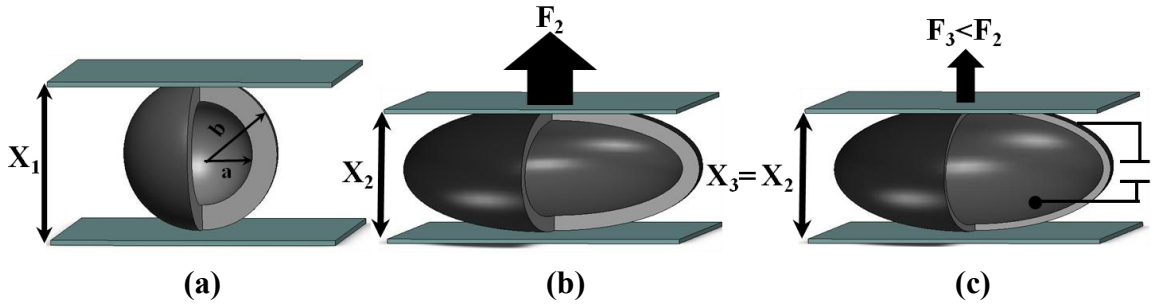

Figure 7-5: Schematic representation of the BSA activation under compressive load test procedure steps: a) Inflated balloon; b) vertically compressed balloon; c) electrically actuated balloon for a fixed displacement $X_3 = X_2$

To characterize the performance of the actuator, seven different prototypes were tested. The manual manufacturing procedure did not allow the reproduction of prototypes having the same dimensions–tested balloons had diameters in the range 65 mm to 97 mm when inflated. The input voltage was generated by a simple code created in LabView

environment and provided to the balloon-shape actuator through a data acquisition (DAQ) device (NI USB-6008) connected via a voltage regulator (National Semiconductor, LM317T) to a high voltage dc converter (EMCO Q101).

Figure 7-6 shows experimental results obtained when the balloon-actuator was kept in a vertically deformed configuration; when no voltage was applied to the balloon electrodes under this position constraint, its reaction force was measured to be about -3.4 N (see Figure 7-6 at time=0s), where the negative sign indicates compressive reaction force recorded by the Microtester instrument.

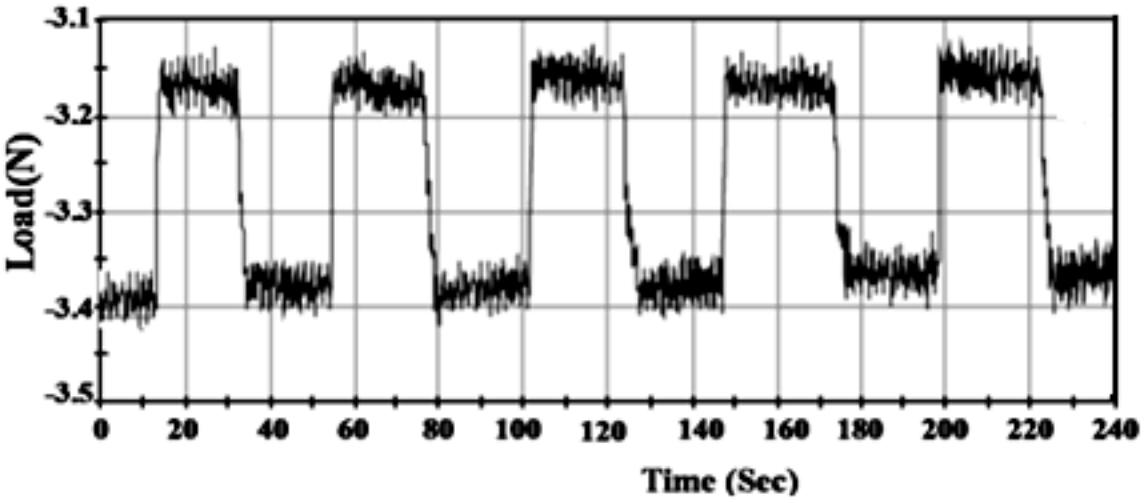

Figure 7-6: Force measurement performed under constant vertical displacement and electrical activation with a square-function voltage input [40].

The balloon was subsequently actuated by applying 10 kV at its electrodes, and a force drop was recorded as expected (about -3.15N in Figure 7-6 at time=20 s); we used 10 kV because this was the maximum voltage bearable by the actuator before voltage breakdown.

In another series of tests we used sinusoidal voltage as input. Figure 7-7 and Figure 7-8 show two different cases in which the same applied voltage, oscillating between 2.4 kV and 10 kV with a period of 125 s, was applied to a balloon prototype. The results shown in Figure 7-7 and Figure 7-8 were obtained by imposing two different initial vertical compression values applied by the Microtester instrument, which were respectively equal to -5.85 N (initial value in Figure 7-7) and -11.85N (initial value in Figure 7-8). These figures show that a higher initial compression of the balloon yielded a higher force variation provided by the actuator for the same value of input voltage (force variation in Figure 7-8 is higher than that in Figure 7-7).

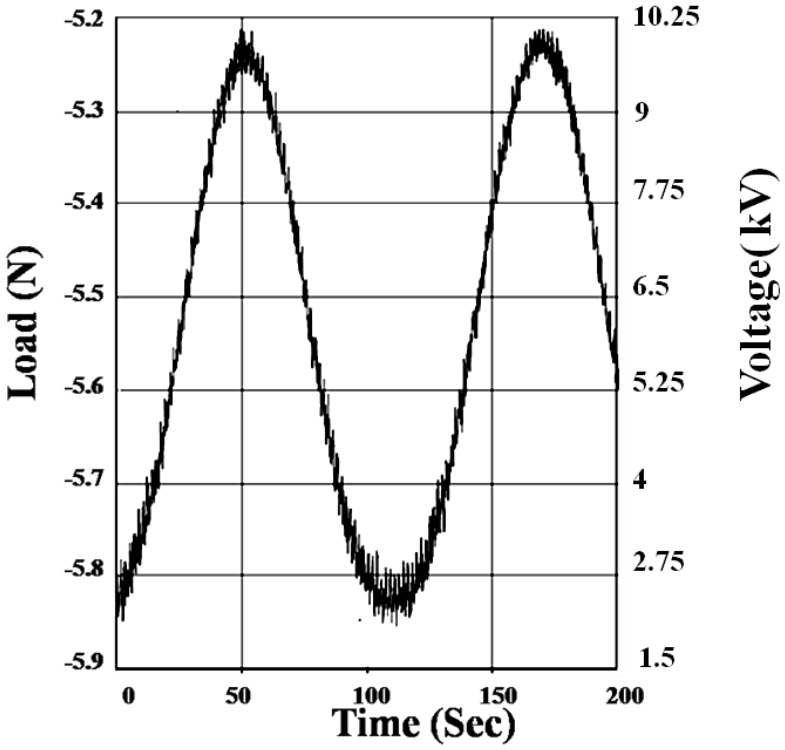

Figure 7-7: Measured force of actuated balloon after applying -5.85 N [40].

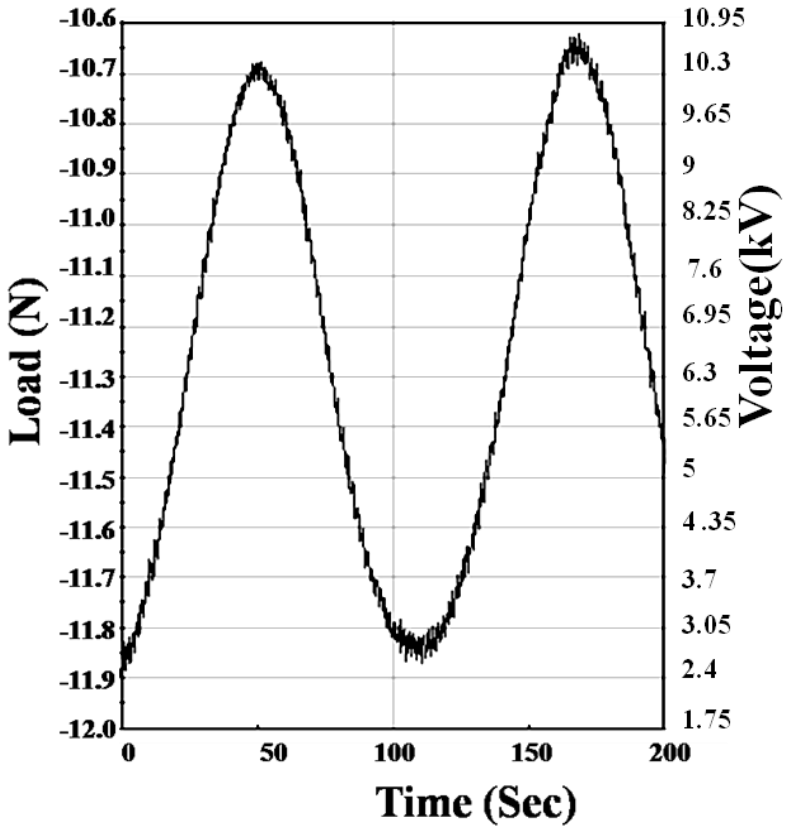

Figure 7-8: Measured force of actuated balloon after applying -11.95 N [40].

Systematic tests were performed to identify the relationship between balloon deformation and force exerted by the balloon when it was electrically actuated. Figure 7-9 shows the two curves representing minimum and maximum forces obtained by applying 10 kV and 0 V to a balloon-shape actuator, which had an initial diameter (D_0) of 97 mm, for different fixed displacements X2 (see Figure 7-5-b,c) imposed by the Microtester instrument. The solid line in Figure 7-9 represents the force applied by the balloon when different constant displacements, X2, were imposed and no voltage was applied to the balloon's electrodes, whereas the dashed line represents the force applied by the balloon when 10 kV was applied.

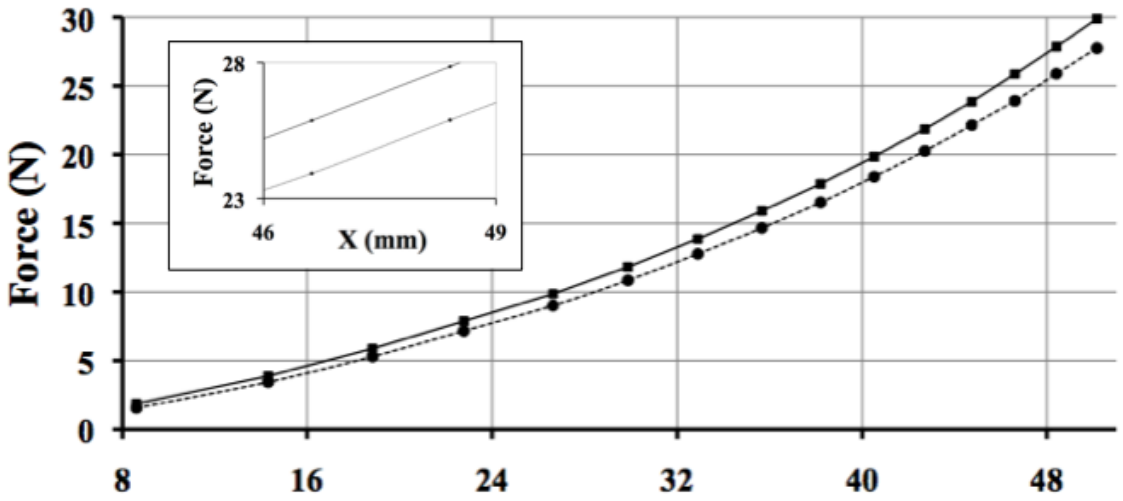

Figure 7-9: Force-displacement relationship for 0 kV (solid line) and 10 kV (dashed line) input [40].

Note that this actuator was designed to exhibit relatively large deformation when loaded with high forces. Figure 7-9 could therefore be misleading because it shows variation of force for fixed displacements. However, this figure also indirectly provides the displacement that an actuator can exert when a constant force is applied. In fact, by tracing a horizontal line in Figure 7-9, which corresponds to a certain constant fixed force, two points intersecting the solid and dashed lines respectively can be determined; these two intersecting points provide the minimum displacement when voltage is not applied (X_{0kV}) and the maximum compression displacement when a voltage of 10 kV is applied (X_{10kV}). Based on results presented in Figure 7-9, a new plot could therefore be obtained representing ΔX, defined as the difference between X_{0kV} and X_{10kV}, versus force. Note that ΔX is equal to the variation of the balloon diameter in the vertical direction, namely ΔD (X1-X2 in Figure 7-5).

Figure 7-10 shows the curve derived from Figure 7-9 following the above-mentioned procedure. This figure is of particular interest as it shows the displacement that this

specific balloon can provide when electrically actuated with 10 kV under a given load. For instance, the actuator would be able to lift a load of 30 N by displaying an active relative displacement of about 2.3%. Because the total mass of this actuator was about 25 g, the force per mass exerted by the actuator was approximately 1.2 N/g.

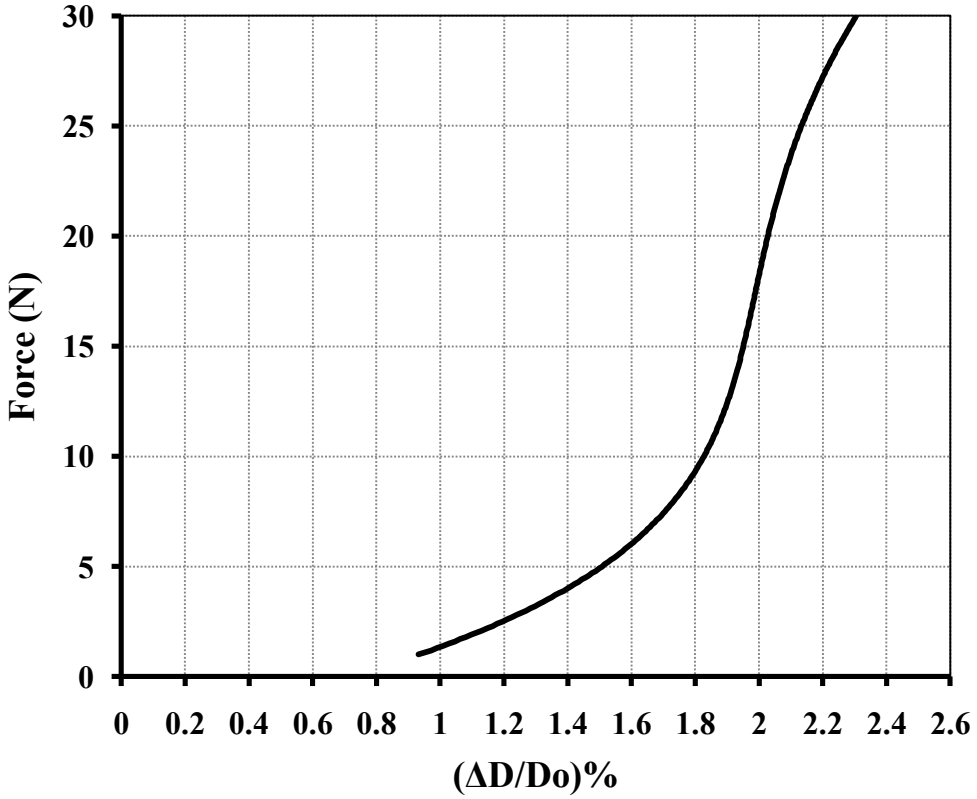

Figure 7-10: Relationship between force and relative diameter displacement when 0kV and 10kV are applied to the balloon's electrodes. The sample considered had initial diameter, D0, equal to 97 mm [40].

Figure 7-11 shows average and standard deviation computed from results obtained by seven tested prototypes; the maximum force in this figure is limited to 8 N because only a few prototypes were able to exceed this value. Most of the failures were caused by rupture of the bonding between the two flat-polymer edges, which were connected to obtain an initial cylindrical shape of the actuator–see section 6.1.1 for details. The results

confirmed that the balloon-shape actuator can display the largest active deformations when subjected to the highest admissible loads.

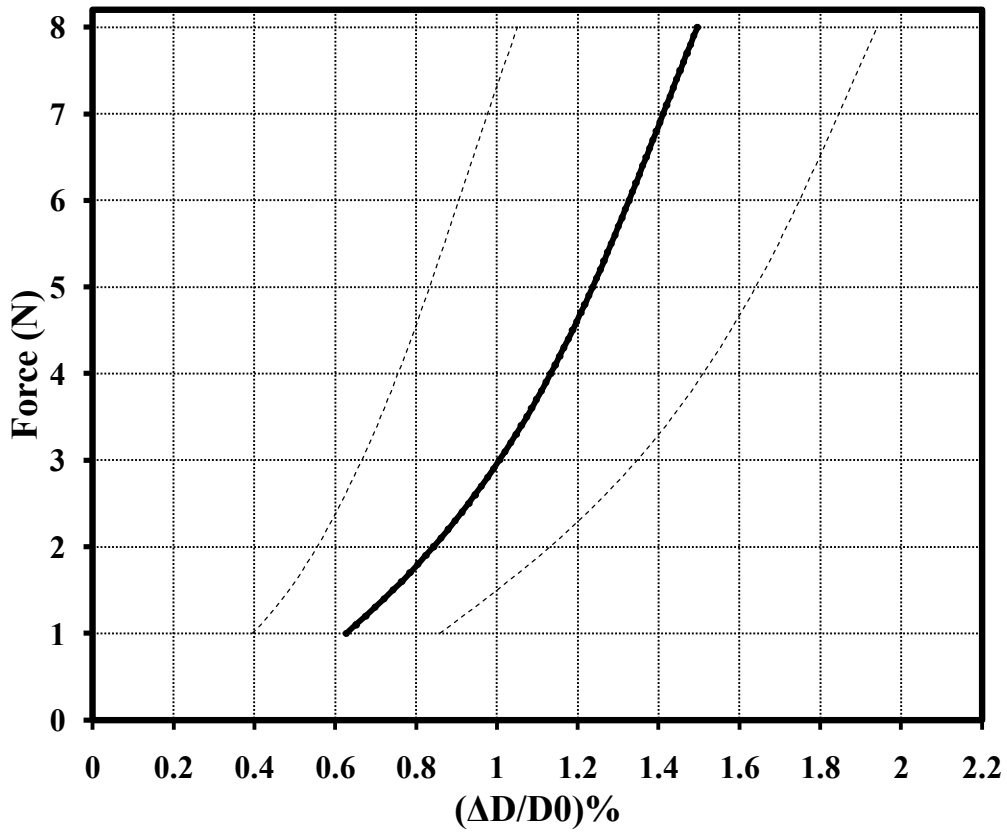

Figure 7-11: Relationship between force and relative diameter displacement when 0 kV and 10 kV are applied to the balloon's electrodes. Different samples were considered. Solid line represents the average. Dashed lines represent the standard deviation [40].

8: Application of a Half BSA for Actuating a Pattern Reconfigurable Square Ring Patch Antenna

In this chapter, we address the last objective of this thesis, namely investigating the use of the BSA for wireless communication applications. Specifically, a compact and cost-effective half BSA (hBSA) is proposed for actuating a Pattern Reconfigurable Square Ring Patch Antenna.

DEAs have recently been introduced as low-cost, compact, easy-to-manufacture actuators for mechanically reconfigurable antennas. Especially, as we show, DE balloon shape actuators demonstrate high force-to-mass ratio.

8.1 Pattern-reconfigurable antenna

The prototype antenna comprises a copper square ring patch [8-9] in the xy-plane (see Figure 8-1) with inner and outer side lengths of 52 mm and 81 mm, respectively, at a height (z-direction) of 4.5 mm from a 180-mm ×180-mm copper groundplane. Styrofoam blocks are used to support the patch's air substrate. A square copper parasitic plane is located in the middle of the ring patch; its side length is 51.2 mm and its thickness is 1 mm.

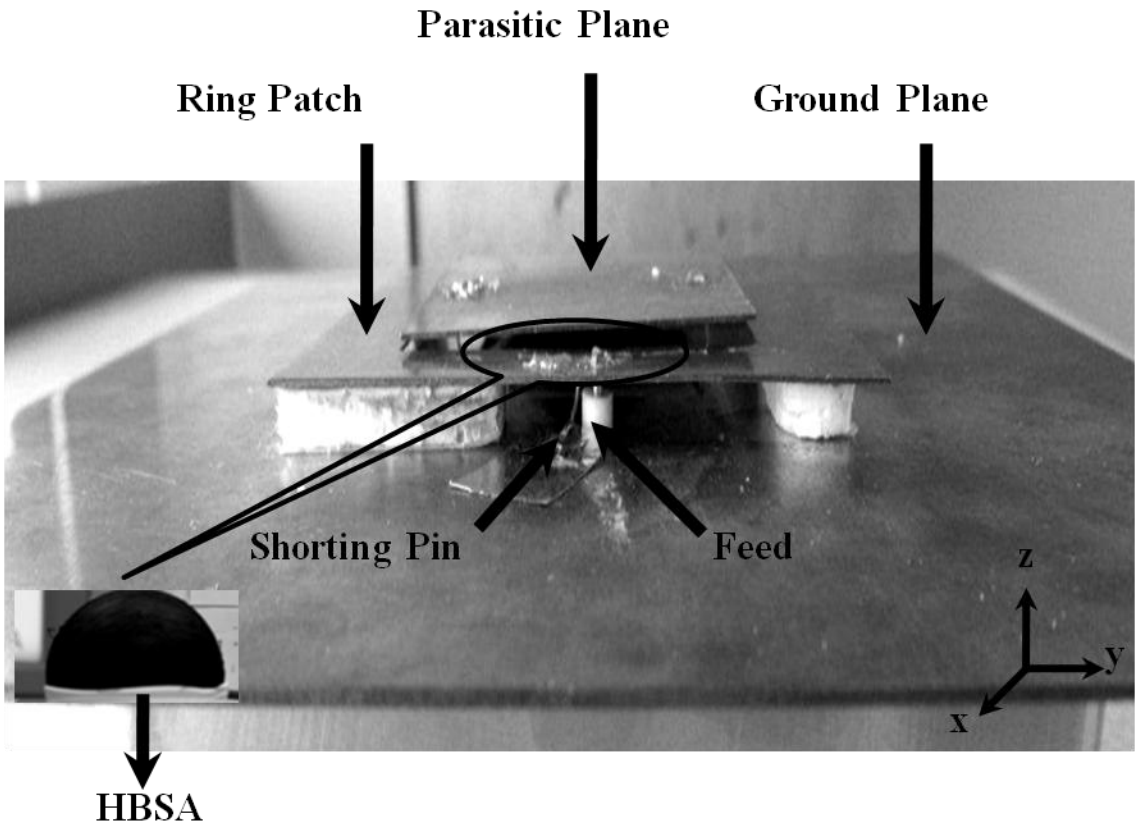

Figure 8-1: Antenna and hBSA set up showing different parts and assembly. The reservoir for pressurized air that is placed under groundplane is not shown.

The parasitic plane is shorted to the groundplane with two shorting pins 1 mm thick (see Figure 8-1). A square slot with a side length of 38 mm is cut out of the middle of the groundplane to provide space for the hBSA. The parasitic plate is kept parallel to the groundplane and ring by its adhesion to the hBSA. Both the antenna and the parasitic plate are electrically isolated from the hBSA and its DC control circuitry. To help attain matching, a shorting pin 1 mm thick is placed at x = 0.5 mm and y = 31 mm from the centre of the ring patch, as shown in Fig.3. The coaxial feed point is placed at a 3-mm distance along the x-axis from this shorting pin, that is, the coax feed is at (x = 3.5 mm and y = 31 mm).

8.2 Fabrication of a half balloon-shape actuator (hBSA)

An hBSA provides a light-weight (~2g) and potentially very low-cost solution for vertical and radial displacements. The fabrication steps of the hBSA used in the prototype antenna are as follows. First, flat DE samples were prepared as explained in section 4.1.1. Two electrodes, consisting of a silicone and carbon-black mixture (see section 4.1.2), are painted on both sides of the flat elastomer. The painted elastomer is then constrained to the top of a cylindrical plastic reservoir of radius (r) equal to 32 mm. By pressurizing the reservoir with air, the elastomer stretches until it buckles and forms a hemisphere on top of the reservoir. The parasitic conductor plate is placed on top of the elastomer to complete the mechanical reconfigurable structure, as shown in Figure 8-1 and Figure 8-2.

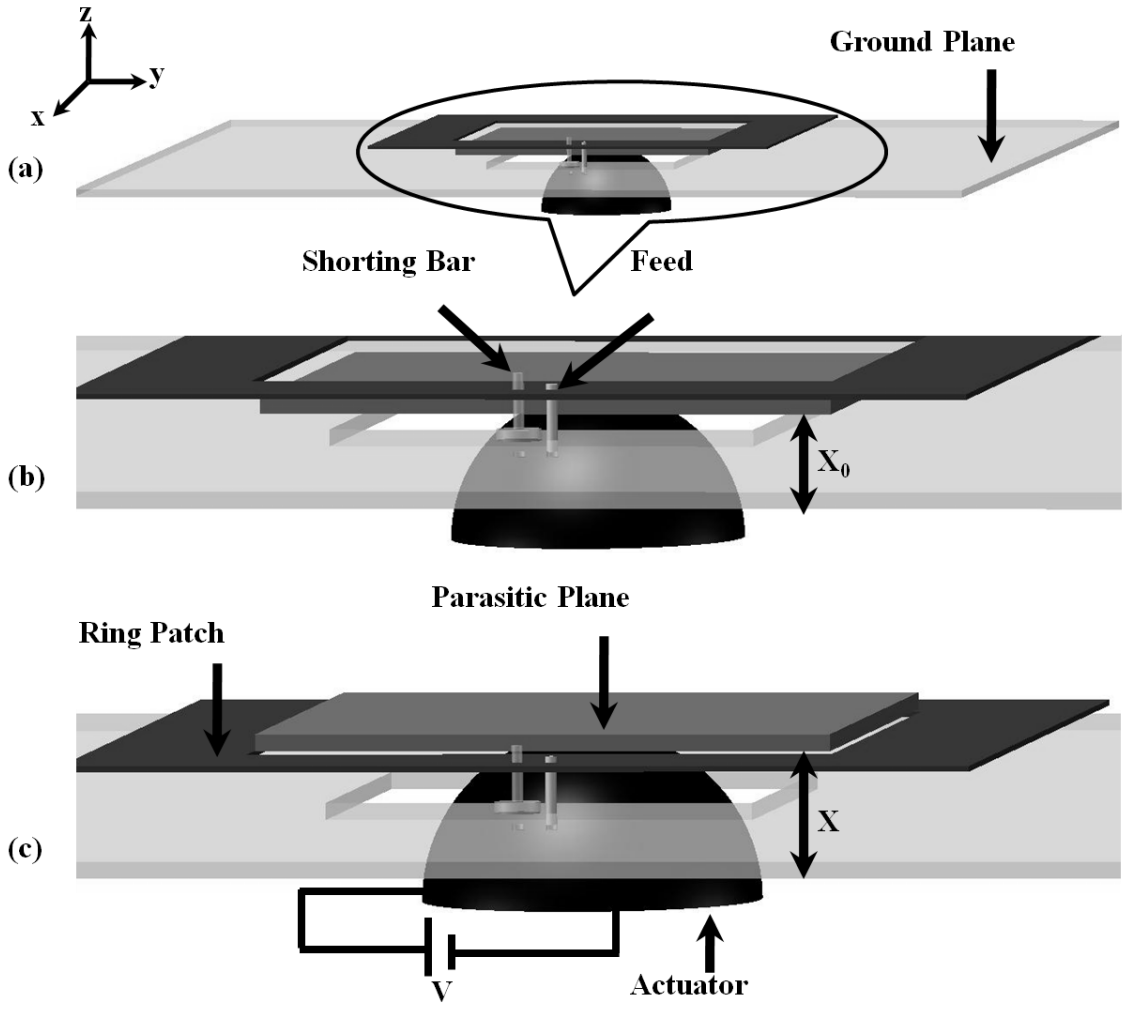

Figure 8-2: Overall schematic representation of the antenna and actuator set up (a) closed up representation of the set up before actuation (b) after actuation (c).

8.3 Experimental result

The hBSA obtained is placed in contact to a parasitic conductor plane and is activated by applying an electric field using a high-voltage DC-DC converter (EMCO-Q101). The electric field causes a radial expansion in the actuator, and as a result, the position of the parasitic plane varies, as shown schematically in Figure 8-2. In this figure, X_0 donates an initial distance between the ground plane and the parasitic plane when the hBSA is not electrically activated, and X is the distance when the hBSA is electrically activated.

Figure 8-3 presents experimental results of the normalized displacement X/X_0 versus the applied electric field. These results were obtained by post-processing high-resolution images taken during hBSA electrical activation.

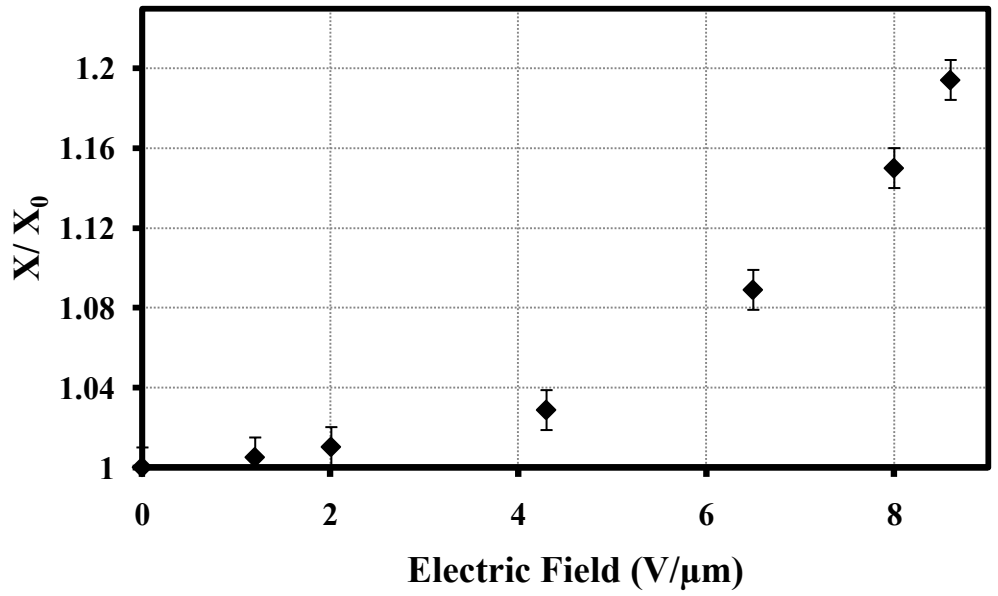

Figure 8-3: The relationship between applied voltage and average relative displacement of the parasitic plane for different dielectric samples

Figure 8-4 depicts the elevation pattern cuts against parasitic height along the *z* axis of experimental results obtained throught the use of a Satimo anechoic chamber. It can be seen that hBSA moved the parasitic plane either below, level with, or above the ring patch, which caused change in antenna pattern.

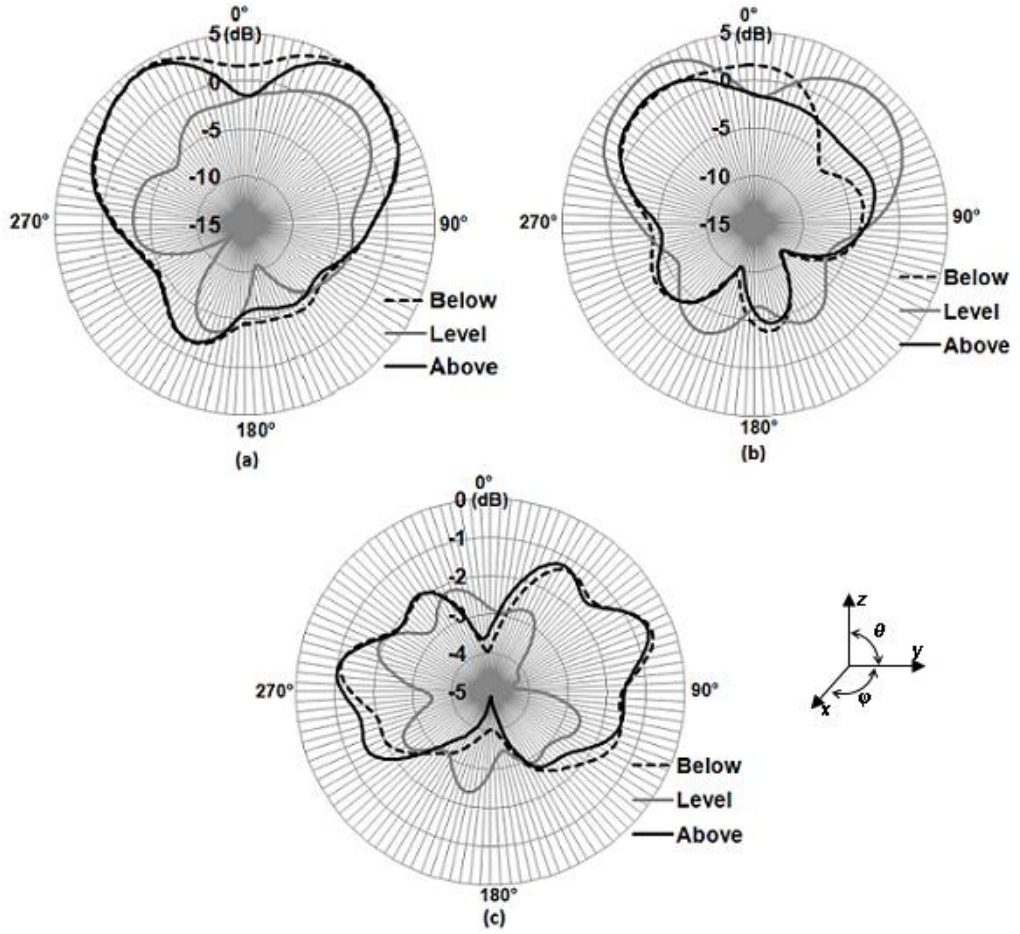

Figure 8-4: Pattern measuremet results from a Satimo chamber against parasitic height (along the *z* axis) for the operation frequency of 1.5 GHz.

9: Conclusion and future work

The study of DEAs is a growing field of research, offering enticing challenges and numerous opportunities. This thesis explores a new actuating technique based on DE and seeds ideas that may expand and bring new discoveries in the future. In this chapter, we summarize and highlight the main results from the thesis.

The development and application of future DEAs require new high-performance actuators that are lightweight, compact, mechanically simple, and inexpensive. DEAs showed good overall performance compared with other existing actuators. A general overview of EAPs, specifically DEAs, and the operational principals was presented in this thesis by reviewing the literature on DEA materials and their modelling.

In this work, a balloon-shape actuator based on DE was investigated in detail and a novel actuation modality proposed. Two case studies were considered to characterize the properties of the proposed BSA. In the first, we characterized the deformation of the BSA by analytically modelling the actuator when inflated (large-deformation analysis) and when electrically activated (small-deformation analysis). In the second study, the BSA behaviour under applied compressive load was investigated experimentally while the BSA was subjected to an electric field.

Acrylic and silicone elastomers were introduced as widely used DE materials. The properties of the material used for BSA were selected by considering linear elasticity and hyper-elasticity theories. To do this, we selected TC-5005 (BJB,USA) as dielectric elastomer for manufacturing the BSA, which is a soft silicone material commercially

available as a three component product, A, B and C. Bone shape samples of the elastomer were prepared and used in tensile tests which resulted in Young's modulus of 44700 Pa for the linear elastic case. For three hyper-elastic models, namely, Neo-Hookean, Mooney-Rivlin, and Ogden, experimental results showed that the Ogden model can fit the entire range of experimental measurements. However, because the maximum deformation of the balloon was less than 200%, the Mooney-Rivlin model was chosen for modelling the BSA as it well fitted the experimental results and was simpler than the Ogden model. Results of the experimental tests showed that for larger applied loads, the strain of the DEA grows faster with increasing voltage. Moreover, it was concluded that the stiffness of the planar DEA was reduced by increasing activation voltage under loads.

We studied the electromechanical behaviour of the BSA and derived mechanical and electrical equations for the balloon-shape actuator, considering nonlinear behaviour for large deformation due to inflation and linear elasticity for small deformation due to electrical activation of the BSA. The small deformation analysis has been validated by a finite element modelling method using ANSYS.

In this work, two manufacturing methods of the BSA were implemented. A new manufacturing method for DEA with spherical configuration using a plastic mould was developed to obtain a BSA with an almost homogenous spherical shape. The actuators manufactured by this method were suitable for investigating a large deformation of BSA (Case study I). However, the BSA wall thickness varied by about ± 50 μm, and surface defects prevented electrical activation of the developed prototype (thickness variation and surface defects cause electrical breakdown). Although this issue could have been solved by replacing the plastic moulds with metallic moulds, metallic moulds were not

fabricated because their extremely high cost did not justify the intended proof-of-concept tests. A second simplified procedure was therefore implemented to perform electromechanical tests. We prepared BSAs using this method for running experiments to study BSA actuation under compressive loads (Case study II). The advantage of this method of fabrication is that it is relatively simple and can be applied easily. However, it has been observed in experiments that if the edges were not bonded properly, then electrical break down would occur, causing the actuator to fail. Moreover, obtaining spherical configuration from a cylindrical tube does not give a symmetrically spherical shape.

To develop and test the BSA performance, a set of experiments for two different case studies were presented in which we compared the derived linear and non-linear large deformation analytical models of the BSA. After using the plastic mould, a BSA was manufactured, which was gradually inflated to measure variation in its outer radius. Results show that the non-linear analytical model fits better to the experimental data, with average error of 17%.

We performed experiments to determine the relation between the inner pressure of a cylindrical BSA and its external radius for various voltage differences applied to the actuator's electrodes. To perform these tests, the simplified BSA manufacturing procedue was used. The BSA diameters ranged between 65 and 97 mm and had an average weight of 22 g before inflation. Furthermore, experiments were performed to assess BSA actuation capability under compressive load. Radial deformation of the activated BSA was determined for different applied compressive loads by an indirect measuring procedure. Results show that this actuator was capable of exerting considerable force

when compressed along its radial direction – a maximum force of about 30 N was recorded. Indirect measurements allowed determining that the actuator could display a maximum radial deformation of about 2.3% when 30 N was applied and a voltage variation between 0 and 10 kV was used.

As an application of the proposed actuator in wireless communication, a mechanically reconfigurable ring patch antenna was equipped with a half BSA to alter the position of a parasitic plane in the middle of the ring, thereby altering its radiation pattern. The compact and light nature of the hBSA in addition to its low cost are the interesting characteristics for this type of actuator. The performed experiments showed that the hBSA is a suitable actuator for mechanically reconfigurable antennas, being capable of moving a parasitic patch below, level with, or above the ring patch antenna plane.

The work described here has resulted in the submission of four journal papers. The first published paper presents the preliminary investigation of a balloon-shape actuator based on electroactive elastomers [40], written as part of this work. The second accepted paper presents preliminary investigations on the design and development of a rolling DEA with a bulged cylindrical shape [47]. The actuator is based on an inflated DE cylinder consisting of a series of dielectric elastomer actuator sectors. The third submitted paper concerns a smart DEA cuff. This paper describes the development of a novel smart cuff, which consists of a cylindrical dielectric elastomer actuator capable of applying a constrictive pressure to the wrist. The design of this actuator is based on the simplified manufacturing design method presented in this thesis. The fourth submitted paper focuses on the application of a half BSA for actuating a Pattern Reconfigurable antenna.

Bibliography

[1] Bar-Cohen J., "Electroactive Polymers:Current Capabilities and Challenges," in *SPIE,Smart Structures and Materials*, 2002, pp. 1-7.

[2] Y. Bar-Cohen, "Electroactive Polymer (EAP)Actuators as Artificial Muscles:Reality, Potential, and Challenges," in *SPIE Press*, Bellingham, Washington, 2004.

[3] F. Carpi, P. Chiarelli, A. Mazzoldi, and D. De Rossi, "Electromechanical characterisation of dielectric elastomer planar actuators: comparative evaluation of different electrode materials and different counterloads," *Sensors and Actuators A-Phys.*, vol. 107, pp. 85-95, 2003.

[4] Q. Pei, R. Pelrine, S. Stanford, R. Kornbluh, and M. Rosenthal, "Electroelastomer rolls and their application for biomimetic walking robots," *Synth. Met.*, vol. 135-136, pp. 129-131, 2003.

[5] F. Carpi and D. De Rossi, "Dielectric elastomer cylindrical actuators: electromechanical modelling and experimental evaluation," *Mater. Sci. Eng.*, vol. 24, no. 4, pp. 555-562, June 2004.

[6] F. Carpi and D. De Rossi, "Contractile dielectric elastomer actuator with folded shape," in *In Proc. of SPIE Smart Struct. and Mat.: Electroactive Polymer Actuators and Devices (EAPAD)*, vol. 6168, San Diego (USA), 2006, pp. 99–104.

[7] N. Goulbourne, M. I. Frecker, E. M. Mockensturm, and A. J. Snyder, "Modeling of a dielectric elastomer diaphragm for a prosthetic blood pump," in *In Proc. of SPIE Smart Struct. and Mat.: Electroactive Polymer Actuators and Devices (EAPAD)*, vol. 5051, San Diego (USA), 2003, pp. 319–331.

[8] P Rosset, Samuel Dubois et al., "Microactuators based on ion implanted dielectric electroactive polymer (EAP) membranes," *Sensors and Actuators A: Physical*, vol. 130-131, pp. 147-154, 2006.

[9] M Wissler and E Mazza, "Modeling of a pre-strained circular actuator made of dielectric elastomers," *Sensors and Actuators A*, vol. 120, pp. 184–192, 2005.

[10] F. Carpi, A. Migliore, G. Serra, and D. De Rossi, "Helical dielectric elastomer actuators," *Smart Materials and Structures*, vol. 14, pp. 1210-1216, 2005.

[11] F. Carpi, A Khanicheh, C Mavroidis, and D. De Rossi, "MRI Compatibility of Silicone Made Contractile Dielectric Elastomer Actuators," *IEEE/ASME Transactions On Mechatronics*, vol. 13, no. 3, pp. 370-374, 2008.

[12] P Lochmatter and G Kovacs, "Design and characterization of an active hinge segment based on soft dielectric EAPs," *Sensors and Actuators A*, vol. 141, pp. 577–587, 2008.

[13] R. E. Pelrine, R. D. Kornbluh, and J. P. Joseph, "Electrostriction of polymer dielectrics with compliant electrodes as a means of actuation," *Sensors and Actuators A-Phys.*, vol. 64, pp. 77-85, 1998.

[14] C. Menon, F. Carpi, and D. De Rossi, "Concept design of novel bio-inspired distributed actuators for space applications," *Acta Astronautica*, vol. 65, no. 5-6, pp. 825-833, 2009.

[15] M Wissler and M Mazza, "Electromechanical Coupling in Direct Elastomer Ascuators," *Science Direct, Sensors and Actuators A: Physical*, vol. 138, no. 2, pp. 384-393, August 2007.

[16] E Biddiss and T Chau, "Electroactive Polymeric Sensors in Hand Prostheses," *Science Direct, Medical Engineering and Physics*, vol. 28, no. 6, pp. 568-578, 2006.

[17] R Pelrine, R Kombuluh, and Q Pei, "High-field deformation of elastomeric dielectrics for actuators," *Materials Science and Engineering*, vol. 11, no. 2, pp. 89-100, November 2000.

[18] P Lochmatter, "Development of a Shell-like Electroactive Polymer (EAP)," Swiss Federal Institute of Technology, Mechanical and Process Engineering, Zurich, PhD Thesis p.340, 2007.

[19] G Kofod, "Dielectric Elastomer Actuators," Technical University of Denmark, Department of Chemistry, Copenhagen, PhD Thesis p.139, 2001.

[20] R Perline, Q Pei, R Kombluh, S Stanford, and S Oh, "Dielectric Elastomer Artificial Muscle Actuators: Toward Biomimetic Motion," in *SPIE*, 2002, pp. 126-137.

[21] J Plante, "Dielectric Elastomer Actuators for Binary Robotics and Mechatronics," Massachusetts Institute of Technology, PhD thesis 2006.

[22] R Kornbluh, R Perline, and J Joseph, "Elastomeric Dielectric Artificial Muscle Actuators for Small Robots," in *Proceedings of the Materials Research Society Symposium*, 1995, pp. 119-130.

[23] G Kofod, R Kornbluh, R Pelrine, and P Sommer-Larsen, "Actuation response of polyacrylate dielectric elastomers," in *SPIE Smart Structures and Materials:Electro-Active Polymer Actuators and Devices (EAPAD)*, Newport Beach, 2001, pp. 141-147.

[24] R Zhang, A Kunz, K Gabor, M Silvain, and A Mazzone, "Dielectric Elastomer Actuators for A Portable Force Feedback Device," in *In Proceedings of Eurohaptics*, Muenchen, 2004, pp. 300-307.

[25] R Zhang, "Development of Dielectric Elastomer Actuators and their Implementation in a Force Feedback Interface," Swiss federal Insttitute of Technology Zurich, PhD Thesis 2007.

[26] R Pelrine, R Kornbluh, Q Pei, and J Joseph, "High-Speed Electrically Actuated Elastomers with Strain Greater Than 100%," *Science*, vol. 287, no. 5454, pp. 836 – 839, 2000.

[27] R. Kornbluh et al., "Highfield electrostriction of elastomeric polymer dielectrics for actuation," in *Proceeding of SPIE Smart Structures and Materials: Electroactive Polymer Actuators and Devices (EAPAD)*, vol. Vol. 3669, Newport Beach, California USA, 1999, pp. 149–161.

[28] R. Kornbluh, R. Pelrine, Q. Pei, S. Oh, and J. Joseph, "Ultrahigh strain response of field-actuated elastomeric polymers. In Y. Bar-Cohen, editor," in *Proc. SPIE Smart Structures and Materials: Electroactive Polymer Actuators and Devices (EAPAD)*, vol. 3987, Newport Beach, California USA, 2000, pp. 51–64.

[29] R. Heydt, R. Kornbluh, R. Pelrine, and V. Mason, "Design and performance of an electrostrictive-polymer-film acoustic actuator," *Journal of Sound and Vibration*, vol. 215, no. 2, pp. 297–311, 1998.

[30] R. Heydt, R. Pelrine, J. Joseph, J. Eckerle, and R. Kornbluh, "Acoustical performance of an electrostrictive polymer film loudspeaker," *Journal of the Acoustical Society of America.*, vol. 107, no. 2, pp. 833–839, Feb 2000.

[31] X. Zhang, M.Wissler, B. Jaehne, R. Broennimann, and G. Kovacs, "Effects of crosslinking, prestrain, and dielectric filler on the electromechanical response of a new silicone and comparison with acrylic elastomer," *Smart Structures and Materials: Electroactive Polymer Actuators and Devices (EAPAD)*, vol. 5385, pp. 78–86, 2004.

[32] G Kofod and P Sommer-Larsen, "Silicon dielectric elastomer actuators: Finite-elasticity model of actuation," *Sensors and Acuators*, vol. 122, pp. 273-283, 2005.

[33] N Goulbourne, E Mockenstrurm, and M Frecker, "A Non-linear Model for Dielectric

Elastomer Membranes," *Journal of Applied Mechanics*, vol. 72, pp. 899-906, 2005.

[34] P Lochmatter, S Michel, and G Kovacs, "Electromechanical model for static and dynamic activation of elementry dielectric elastomer actuator," in *SPIE*, 2006, pp. 1-13.

[35] A Tews, K Pope, and A Snyder, "Pressure-volume characterriestics of dielectric elastomer diapheragms," in *SPIE*, San Diego, 2003, pp. 159-169.

[36] Q Pei, R Rosenthal, S Stanford, and Kornbluh, "Multifunctional electroelastomer roll actuators and their application forbiomimetic walking robots," in *Proc. of SPIE Smart Struct. and Mat.:Electroactive Polymer Actuators and Devices (EAPAD)*, San Diego (USA), 2003, pp. 281-290.

[37] J Plante and S Dubowsky, "Large-scale failure modes of dielectric elastomer actuators," *International Journal of Solids and Structures*, vol. 43, pp. 7727-7751, March 2006.

[38] J Plante and Steven Dubowsky, "Large-scale failure modes of dielectric elastomer actuators," *International Journal of Solids and Structures*, vol. 43, pp. 7727-7751, March 2006.

[39] F. Carpi, C. Menon, and D. De Rossi, "Electroactive Elastomeric Actuator for All-Polymer Linear Peristaltic Pumps," *IEEE Transactions on Mechatronics,Volume. PP (2009)*, no. 99, pp. 1-11, 2009.

[40] M Soleimani and C Menon, "Preliminary investigation of a balloon-shape actuator based on electroactive elastomers," *Smart Materials and Structures*, vol. 19, p. 6pp, 2010.

[41] R Pelrine and R Kornbluh, "Variable-stiffness-mode dielectric elastomer devices," *Advances in Science and Technology*, vol. 61, pp. 192-201, 2008.

[42] L Lerner, *Physics for scientists and engineers,volume 2*, 705th ed. London, UK: Jones and Barllet publishers, 1995.

[43] R Ogden, *Non-Linear elastic Deformations*. Toronto, Canada: General publishing, 1997.

[44] A Ibrahimbegović, *Nonlinear Solid Mechanics: Theoretical Formulations and Finite Element*.: Springer, 2009.

[45] A Bower, *Applied Mechanics of Solids*.: CRC press, 2010.

[46] J Heinbockel, *Introduction to Tensor Calculus and Continuum Mechanics*, 255258th

ed. Norfolk, Virginia: Old Dominion University, Norfolk-Virginia, 1996.

[47] S Timoshenko, *Theory of Elasticity*, Third Edition ed. Singapore: McGraw-Hill press, 1982.

[48] Marco Potz et al., "Rolling dielectric elastomer actuator with bulged cylindrical shape," *Smart Materials and Structures*, vol. 19, no. 12, 2010.

[49] J Zhu, S Cai, and Z Suo, "Nonlinear oscillation of a dielectric elastomer balloon," *SCI:Polym Int*, vol. 59, pp. 378-383, 2010.